Seasonal inhomogeneity in cloud precursors over Gangetic Himalayan region during GVAX campaign

U. C. Dumka[1*], Deepika Bhattu[2], S. N. Tripathi[2], D. G. Kaskaoutis[3], and B. L. Madhavan[4]

[1]Aryabhatta Research Institute of observational sciences (ARIES), Nainital, India

[2]Department of Civil Engineering, Indian Institute of Technology, Kanpur, India

[3]Department of Physics, School of Natural Sciences, Shiv Nadar University, India

[4]Leibniz Institute for Tropospheric Research (TROPOS), Germany

[E-mail: dumka@aries.res.in; dimitris.kaskaoutis@snu.edu.in; snt@iitk.ac.in]

Running title: CCN properties over Gangetic Himalayan region

Abstract

Atmospheric aerosols are key elements in cloud microphysics, the hydrological cycle and climate by serving as cloud condensation nuclei (CCN). The present work analyzes simultaneous measurements of number concentration of CCN (N_{CCN}) and condensation nuclei (N_{CN}) obtained at Nainital, in the Gangetic-Himalayan (GH) region, during the frameworks of Ganges Valley Aerosol Experiment (GVAX), June 2011 to March 2012. The N_{CCN}, N_{CN} and activation (AR = N_{CCN}/N_{CN}) at 0.31-0.33% S (supersaturation ratio), exhibit significant daily, monthly and seasonal variations within a range of 684-2065 cm^{-3} for N_{CCN}, 1606-4124 cm^{-3} for N_{CN}, and 0.38-0.60 for AR, suggesting large inhomogeneity in aerosol properties, types and sources, which control the degree of aerosol potential activation. Thus, transported aerosols from the Ganges valley and abroad, the boundary-layer dynamics and atmospheric modification processes play an important role in aerosol-cloud interactions over the GH region. The N_{CN} and N_{CCN} show monthly-dependent diurnal variations with afternoon maxima due to transported aerosols from the Ganges valley up to the Himalayan foothills, while the AR is lower during these hours implying lower hygroscopicities or smaller sizes of the transported aerosols. The dependence of N_{CCN} on S is highest during Dec-Mar and lowest during monsoon (Jun-Sep), suggesting different aerosol chemical composition. Comparison between Nainital and Kanpur shows that N_{CN} and N_{CCN} are much lower at Nainital, while the similarity in AR suggests aerosols of similar type, source and chemical composition uplifted from the Ganges valley to the Himalayan foothills.

Keywords: Cloud Condensation Nuclei, Activation Ratio, transported aerosols, Gangetic Himalayan region, Ganges Valley Aerosol Experiment

*Corresponding Author: Dr Umesh Chandra Dumka, ARIES, Manora Peak, Nainital
E-mail: dumka@aries.res.in; ucdumka@gmail.com

© 2014. This manuscript version is made available under the Elsevier user license
http://www.elsevier.com/open-access/userlicense/1.0/

1. Introduction

Cloud condensation nuclei (CCN) are hygroscopic particles that can activate at various supersaturation (S) levels to cloud droplets. CCN are thus key elements of cloud microphysics, the hydrological cycle and climate from local/regional to global scales (Lohmann and Feichter, 2005). The ability of particles to be CCN strongly depends on their size distribution and chemical composition (Fitzgerald, 1973; Pruppacher and Klett, 1997; Dusek et al., 2006; Lance et al., 2009; Srivastava et al., 2013). Furthermore, cloud microphysical properties, such as cloud-droplet size, cloud albedo and lifetime, cloud-top height and precipitation rate are influenced by the prevailing CCN, thereby affecting the climate system (Twomey, 1977; Pruppacher and Klett, 1997; Ramanathan et al., 2001; Andreae et al., 2004; Rosenfeld et al., 2008). Aerosol-cloud interactions (aerosol indirect effect) are still a significant source of uncertainty in climate modelling and dynamics (IPCC, 2007) due to complicated cloud microphysics phenomena, their impact on radiative properties, precipitation and the hydrological cycle (Andreae and Rosenfeld, 2008). As a consequence, CCN measurements and knowledge of their spatio-temporal evolution are challenging tasks to quantify the aerosol indirect effect on climate.

Over the last few decades, emissions of anthropogenic aerosols and pollutants have dramatically increased over the Indo-Gangetic Plains (IGP), India because of the rapid increase in population, industrialization and urbanization (Lawrence and Lelieveld, 2010; Lu et al., 2011). Despite the availability of numerous studies on aerosol optical, physical and chemical properties over IGP and Gangetic-Himalayan (GH) region (Jethva et al., 2005; Tripathi et al., 2005; Dumka et al., 2008, 2014a; Dey and Di Girolamo, 2010, 2011; Lawrence, 2011; Srivastava et al., 2011; Kaskaoutis et al., 2012), extensive measurements and analysis of CCN are still sparse given their role in cloud formation. Recent studies (Patidar et al., 2012; Srivastava et al., 2013; Bhattu and Tripathi, 2014; Ram et al., 2014) over IGP, using both ground-based and airborne observations, have reported significant seasonal variations of N_{CCN} with maximum during winter and minimum during monsoon. Furthermore, the findings from a recent campaign "Cloud Aerosol Interaction and Precipitation Enhancement Experiment (CAIPEEX)" constitute an important contribution to this research over a climatically sensitive area, where the onset, intensity and duration of the monsoon affect climate, ecosystems and the economy (Chakravarty et al., 2011; Dipu et al., 2013; Padmakumari et al., 2013).

The current work deals with measurements of condensation nuclei (N_{CN}) and Cloud Condensation nuclei concentrations (N_{CCN}) obtained through the Atmospheric Radiation Measurement-Mobile Facility one (AMF-1) deployed at Aryabhatta Research Institute of observational sciences (ARIES), Nainital (29.4^{o} N, 79.5^{o} E; 1958 m above mean sea level), during the intensive field campaign Ganges Valley Aerosol Experiment (GVAX; Manoharan

et al., 2014; Dumka and Kaskaoutis, 2014; Dumka et al., 2014b). Air mass back-trajectory analysis via the Hybrid Single Particle Lagrangian Integrated Trajectory (HYSPLIT; Draxler et al., 2012) model and variations in boundary-layer height are examined to investigate the role of transported aerosols and upslope airflows on aerosol-cloud interactions over Nainital. Moreover, simultaneous measurements of N_{CCN} and N_{CN} obtained in Kanpur, located in the central IGP, during June-August of 2011 are also analysed and compared with those at Nainital to explore the spatio-temporal and altitude dependent CCN properties over the GH region.

2. Observation Site, Instruments and Data

2.1. Site Description and Meteorological Parameters

In-situ measurements of N_{CCN} and N_{CN} were carried out during June 2011 to March 2012 at ARIES, Nainital, which is an elevated (1958 m) site located in the central Himalayan region approximately ~ 300 km northeast of New Delhi (Fig. 1). Nainital, with negligible industrial activity and a population of about half a million (census of 2011), is an excellent site for monitoring background aerosol concentration as well as long-range transported aerosols (Dumka et al., 2010, 2011).

Weather conditions at this site can be classified into four seasons: winter (DJF; December-February), pre-monsoon (MAM; March-May), monsoon (JJA; June-August) and post-monsoon (SON; September-November) (Dumka et al., 2010). During the frameworks of the GVAX campaign, the average wind speed was 2.33 ± 1.75, 2.02 ± 1.39, 2.26 ± 1.49 and 1.83 ± 1.28 m s^{-1} during winter, pre-monsoon (only March data), monsoon and post-monsoon, respectively. Northwesterly stronger winds that dominated most of the time (late post-monsoon to March) are responsible for the transport of air masses from arid/semi-arid regions of northwestern India, Pakistan and west Asia (Jaidevi et al., 2011). The percentage of southeasterly monsoon winds increased during the monsoon, and continued to be high during September, leading to heavy rains and aerosol washout. During the post-monsoon, stable atmospheric conditions prevailed over the site, while in winter, western disturbances favoured some rain and/or snowfall in January and February. Seasonal temperature (in ^{o}C) ranged from 17 to 26 (with mean 20 ± 2) in JJA; 9 to 26 (17 ± 3) in post-monsoon; 0 to 24 (10 ± 4) in winter and 4 to 27 (15 ± 5) in March. The average relative humidity (RH in %) was highest during the monsoon (> 90%) and minimal (~ 45%) during March, while rainfall from June to September accounted for more than 85% of the total rainfall during the study period.

2.2. Condensation Nuclei (CN) and Cloud Condensation Nuclei (CCN) measurements

N_{CCN} and N_{CN} were measured by the Atmospheric Radiation Measurement (ARM) Aerosol Observing System (AOS; Jefferson, 2011; Dumka and Kaskaoutis, 2014; Dumka et

al., 2014b), which is the primary platform used for in-situ aerosol measurements at the surface. The number concentration of CN was measured by a butanol based Condensation Particle Counter (CPC; TSI Model 3010), which is a compact and rugged instrument that measures N_{CN} in diameter range 0.01-3.0 μm. The particles are allowed to grow large enough to be counted with a simple optical particle counter in the presence of butanol. The supersaturation ratio of butanol vapour in the condenser controls the minimum detectable particle size range of the counter. The instrument has a high signal-to-noise ratio that attains accurate detection of small particles. The upper concentration limit of the CPC is 10,000 particles per cubic centimetre.

N_{CCN} were measured by a Droplet Measurement Technology (DMT) continuous flow single column CCN Counter [CCNC; Roberts and Nenes, 2005; Lance et al., 2006; Rose et al., 2008). It measures activated particle concentrations being converted to cloud droplets by condensation of water at a given S. According to the Köhler equation, the vapor pressure or S above an aqueous drop will vary with let drop surface tension and size and the solute concentration or chemical composition. During GVAX, the S of the CCN counter was stepped through 7 intervals with 5 minutes at each setting (Jefferson, 2011). The S on the CCN datastream is calculated using a heat transfer and fluid dynamics flow model (Lance et al., 2006; Jefferson, 2010, 2011; and reference cited therein). The fluid dynamic flow model uses the calibrated temperatures, pressures, and flows within the instrument to calculate the S. Changes in S are due to changes within the column thermal properties of the instrument. This CCN counter was calibrated at the beginning and end of the campaign (Jefferson, 2010, 2011; http://www.arm.gov/publications/tech_reports/handbooks/aos_handbook.pdf).

N_{CCN} measurements were considered at 5-min intervals (1-min measurements averaged into 5 min) for each S level, while N_{CN} were measured continuously (1-min time interval, also averaged for 5 min) by the CPC. This procedure leads to ~41 different set of measurements per day, which then were averaged on daily, monthly and seasonal basis. The N_{CN} measurements used in the analysis are compared with those of N_{CCN}, since they were averaged at the same time intervals as the N_{CCN} measurements for each S level.

In order to compare N_{CN} and N_{CCN} concentrations between GH and IGP regions, simultaneous measurements of N_{CN} and N_{CCN} were performed in Kanpur (independent of the GVAX campaign). Following methodology given by Lathem and Nenes (2011), a supersaturation depletion correction was applied to the Kanpur datasets, while the CCN counter has been calibrated before and after the deployment. Details of the measurement protocol at Kanpur, data analysis methods, instrument calibration, accuracy and errors are presented elsewhere (Patidar et al., 2012; Srivastava et al., 2013; Bhattu and Tripathi, 2014; Ram et al., 2014).

3. Results and Discussions

3.1. Temporal variation of N_{CN}, N_{CCN} and Activation Ratio (AR)

Figure 2 shows the daily-averaged values of N_{CCN}, N_{CN} and AR at four S (0.17-0.22%, 0.31-0.33%, 0.46-0.48% and 0.75-0.78%) levels at Nainital during the GVAX field campaign. The vertical solid line separates the S levels for June to September 2011 (left) from those during November 2011 to March 2012 (right). Unfortunately, the N_{CN} measurements were not available in October 2011 due to instrument technical problems. Significant temporal variations are seen during the entire period with daily-averaged N_{CN} ranging from 684 - 5479 cm^{-3} (mean ± 1σ of 2630 ± 969), 702 – 6555 cm^{-3} (2873 ± 1162), 687 - 8183 cm^{-3} (3193 ± 1467) and 282 – 9916 cm^{-3} (3588 ± 1978) at 0.17-0.22%, 0.31-0.33%, 0.46-0.48% and 0.75-0.78%, respectively. The slight increase in CN at higher S is an artifact of the time-sampling differences between CN and CCN at different S and it would bias diurnal trends and spectral plots. The corresponding N_{CCN} are on the order of 9-2180 cm^{-3} (mean ± 1σ of 800 ± 437), 24-3649 cm^{-3} (1421 ± 728), 44-5411 cm^{-3} (1844 ± 973) and 97-6414 cm^{-3} (2138 ± 1260), respectively, which are typical for the GH region (Gajananda et al., 2005; Komppula et al. 2009; Sellegri et al. 2010; Moorthy et al., 2011; Hyvärinen et al., 2011); σ corresponds to the standard deviation of the means over the whole measuring period. N_{CCN} increases significantly with S implying numerous small particles. The monthly statistics of N_{CCN}, N_{CN} and AR at 0.31-0.33% S are listed in Table 1. The large differences between maximum and minimum values (~$3x10^3$ cm^{-3} for N_{CCN} and ~$5x10^3$ for N_{CN}) are indicative of the large variation of CCN and CN over the observation site. The highest monthly values of N_{CCN} (2065 ± 476 cm^{-3}) and N_{CN} (4124 ± 747 cm^{-3}) are observed in March, while the corresponding minimum (684 ± 396 cm^{-3} and 1606 ± 453 cm^{-3}) in August. The minimum N_{CN} monthly-mean value is slightly higher than that reported at Hanle, a high-altitude (5000 m amsl) station in the northwestern arid trans-Himalayan region. The N_{CN} at Hanle during August to November 2009 varied between 80 and 8000 cm^{-3}, with median and mean values of ~ 950 cm^{-3} and 1150 ± 500 cm^{-3} (Moorthy et al., 2011). This suggests that the Nainital site is under the influence of increased loading of mostly transported aerosol plumes from the IGP, which cannot cross the mountainous range and affect Hanle located in the lee (northern) slopes of the Himalayas.

The N_{CN} values are somewhat comparable to those reported for another high altitude (2180 m amsl) site at Mukteshwar (3108 ± 1570; 4010 ± 1965; 3195 ± 2683 and 2124 ± 1234 cm^{-3}, respectively for the years 2006, 2007, 2008 and 2009, Komppula et al., 2009) and about an order of magnitude lower than those (25860 ± 11707 cm^{-3}) observed over the polluted Gual Pahari site (243 m amsl in the IGP) during the year 2009 (Hyvärinen et al., 2011). Based on three years of continuous measurements in Mukteshwar (close to Nainital), Komppula et al. (2009) reported that the monthly averages of the total aerosol number

concentration varied from ~5700 cm^{-3} to ~1200 cm^{-3} from pre-monsoon to monsoon. Measurements at the high altitude (5079 m amsl) Nepal Climate Observatory-Pyramid, (Sellegri et al., 2010) have shown annual average aerosol number concentration on the order of 860 ± 55 cm^{-3}, exhibiting a strong seasonal variation with pre-monsoon and post-monsoon high (~ 1500 cm^{-3} and 1300 cm^{-3}) and monsoon low (~ 450 cm^{-3}). Since, the Pyramid is a remote site in the Everest area, the observed aerosol is mostly transported from the Indian polluted regions, while the annual pattern of N_{CN} is a combination of the IGP aerosol variability and boundary-layer dynamics (Sellegri et al. 2010). On the other hand, airborne studies have shown significant vertical heterogeneity in N_{CN} over the GH region, influenced by local emissions (mostly within the boundary layer), long-range transport (mostly at higher altitudes) and changes in mixing height (Dipu et al., 2013; Padmakumari et al., 2013; Srivastava et al., 2013). Airborne profiles during the CAIPEEX campaign in May 2009 have shown surface concentrations of 1100 - 1500 cm^{-3} and 800 - 1600 cm^{-3} at higher elevations (between 2 and 4 km) over Pune, while the respective concentrations over Pathankot (a site in the GH region) were in the range of 1300 – 2800 cm^{-3} at the surface and 2500 - 6800 cm^{-3} at higher altitudes (between 2 and 4 km) (Padmakumari et al., 2013). The higher N_{CN} over the GH region is attributed to the influence of dust plumes from the Thar Desert and southwest Asia that also affect Nainital during the pre-monsoon season. The aerosol profiles revealed a nearly homogeneous vertical layer up to 3-4 km with concentrations of ~800-1700 cm^{-3} and a decrease afterwards over Bareilly site in the IGP, just south of Nainital (Padmakumari et al., 2013). Using long-term (January 1996 to December 2003) analysis, Gajananda et al. (2005) have studied the aerosol number concentration at three altitude levels (1150, 2050 and 2530 m amsl) in the northwestern Indian Himalayas reporting mean concentrations ranging from 4352 to 1392 cm^{-3} from the lowest to highest level, respectively. The above comparisons, as well as the comparison between Nainital and Kanpur (see section 3.7), reveal that the observing site is located at an intermediate zone between the polluted IGP and the mostly clean Himalayan range.

The N_{CCN} is much lower during the monsoon months because of high precipitation and washout of the suspended particles. Similar annual variation (winter high and monsoon low) was found in Kanpur (Patidar et al., 2012), but with much higher N_{CCN} values compared to Nainital. Based on aircraft measurements over Kanpur, Srivastava et al. (2013) reported high values of N_{CCN} at S = 0.84%, such as 5293 ± 978 cm^{-3} and 4431 ± 1552 cm^{-3} on 2nd July 2009 (at 10:35-12:25 and 14:15-15:15 hours local time, respectively). High mean values [3523 (0.81), 4572 (0.64) and 2361 (0.36)] of N_{CCN} at S = 0.3% were also reported for March, May-June and August, respectively over Kanpur (Bhattu and Tripathi, 2014); the values in parenthesis are the AR for the respective periods.

Similar to N_{CCN} and N_{CN}, the AR exhibits significant temporal variation in its daily mean values (Fig. 2), ranging from 0.01 to 0.67 (mean of 0.32 ± 0.13), 0.03 to 0.77 (0.51 ± 0.13), 0.06 to 0.78 (0.58 ± 0.12) and 0.03 to 0.80 (0.60 ± 0.14) at 0.17-0.22%, 0.31-0.33%, 0.46-0.48% and 0.75-0.78% S levels, respectively. An AR value close to 1 indicates the presence of aged background aerosol (Andreae and Rosenfeld, 2008), while over the observational site the monthly-mean values are much lower than 1 at 0.31-0.33% S level (Table 1). The highest AR values during November are associated with biomass burning in northwestern India and aged transported aerosol plumes mixed with other organic or inorganic particles that are more hygroscopic (Lee et al., 2010). On the other hand, the observational site is above the planetary boundary layer in winter and, therefore, the aged free tropospheric aerosols may also play a role in the high AR values in that season (Venzac et al., 2009).

The mean values of N_{CN} and N_{CCN} observed at Nainital are higher than those reported during the Indian Ocean Experiment (Hudson and Yum, 2002) and lower than those found over the Korean Peninsula (Yum et al., 2005, 2007). During the Indian Ocean Experiment, Hudson and Yum (2002) found average values of 1808 ± 41 cm^{-3}, 1190 ± 128 cm^{-3} and 0.66 for N_{CN}, N_{CCN} and AR, respectively, at 1.0% S. Very high values of N_{CN} (6444 ± 2732 cm^{-3}, 4644 ± 2454 cm^{-3} and 9804 ± 4142 cm^{-3}) and N_{CCN} (3445 ± 1158 cm^{-3}, 2475 ± 955 cm^{-3} and 3178 ± 1269 cm^{-3}) at 0.49% S during August, September and October, respectively are reported at Shouxian, a polluted site in China (Liu et al., 2011). Aircraft measurements over Nainital on 29th June 2009, revealed average values of 1363 ± 327 cm^{-3} and 18,292 ± 3770 cm^{-3} (0.84% S) for CCN and CN, respectively at the altitude range 518-5486 m (Srivastava et al., 2013). Recently, Konwar et al. (2012) reported N_{CCN} of 1153-2470 cm^{-3} (for the north-eastern part of India on 30th August and 4th-6th September 2009) and 3361-10,635 cm^{-3} (for extremely polluted conditions in the IGP on 14th-25th August 2009) at 0.4% S during the CAIPEEX campaign. Shrestha et al. (2013) have studied the CCN properties over the central Nepal region (Besisahar) and reported mean N_{CCN} of 435 ± 98 cm^{-3} and 750 ± 50 cm^{-3}, during clean and hazy/polluted skies, respectively at S ranging from 0.35% to 0.45%; N_{CCN} at another site (Dhulikhel) in Nepal was found to be 700 cm^{-3} at S = 0.3%. Table 2 summarises the values of N_{CCN}, N_{CN} and AR obtained at Nainital (GVAX campaign) with those measured over high altitude sites over the globe. Asmi et al. (2012) have reported similar value of N_{CCN} at Puy-de-Dome during summer (200-2000 cm^{-3}) and winter (50-3000 cm^{-3}) with N_{CN} up to 10,000 cm^{-3}. The AR (at 0.24% S) ranges between 0.2 and 0.7 at Puy de Dome, which is comparable to that at Nainital. The N_{CN} and N_{CCN} at Mt. Sonnblick (Hitzenberger et al., 1999), Storm Peak Laboratory (Friedman et al., 2013) and Jungfraujoch (Jurănyi et al, 2010) are lower than those obtained at Nainital, since these mountainous sites are far from polluted sources like IGP.

3.2. Diurnal Variation

The mean diurnal variations of N_{CCN}, N_{CN} and AR at 0.31-0.33% S for characteristic months of each season are shown in Fig. 3a-c, respectively. A pronounced diurnal variation of N_{CCN} and N_{CN} is observed in November, December and March with prominent afternoon peaks, whereas the diurnal pattern is smooth and nearly vanished in June. During November to March, N_{CCN} and N_{CN} gradually increase from 08:00 until 15:00-18:00 hours to peak values, and then decrease to nighttime minima. Increased N_{CN} and N_{CCN} and larger variability around noon to early afternoon could be due to nucleation events and new particle formation (Moorthy et al., 2011).

Diurnal patterns for AR are opposite those of N_{CCN} and N_{CN}, with lower values during noon and late afternoon hours and larger values in the morning. The AR diurnal patterns are similar for the months of November and March, while the AR values are much lower in June. Diurnal variations are influenced by the planetary boundary layer dynamics and the mountain-valley winds. The role of mountain-valley breeze (upslope valley winds and downslope mountain winds during daytime and nighttime, respectively) and topography in diurnal variations of near-surface aerosol concentrations and trace gases at high-altitude sites has been well documented (Nishita et al., 2007; Panday and Prinn, 2009; Panday et al., 2009; Shrestha et al., 2010; Dumka et al., 2010; Sellegri et al. 2010; Moorthy et al., 2011; Sarangi et al., 2014). The upslope winds bring relatively polluted air masses from the IGP to the mountain slopes and play an important role in diurnal variations of aerosol over the GH region (Kleissl et al., 2007; Raatikainen et al., 2014). Diurnal patterns of N_{CCN} and N_{CN} are similar to the diurnal variations of the near surface aerosol and black carbon mass concentrations at Nainital (Pant et al., 2006; Dumka et al., 2010) due to uplift of pollutants from the IGP (Raatikainen et al., 2014). In contrast, the diurnal variation of N_{CCN} in Kanpur (Patidar et al., 2012) presents a prominent peak in the morning (~08:00 hours) and a secondary one in the evening (20:00 hours), closely following the diurnal variation of local aerosol emissions and mixing height dynamics (Tripathi et al., 2005). It is, therefore, concluded that both N_{CCN} and N_{CN} are strongly driven by daily aerosol and pollutant variations, of which surface heating, boundary-layer dynamics and long-range transport play a prominent role (Dumka et al., 2013).

3.3. Variations with meteorological parameters

It is well known that $N_{CCN}(S)$ (CCN spectra) depends on aerosol physico-chemical properties, meteorological conditions, and transport processes (Elminir, 2005; Cheng et al., 2008). Therefore, meteorological parameters, such as ambient temperature, surface wind speed and direction, measured by ARM mobile Facility surface meteorology station at 1 min intervals, are correlated with N_{CCN}, N_{CN} and AR during the campaign. The analysis did not reveal a significant correlation of N_{CCN}, N_{CN} and AR with ambient temperature over the site,

even during periods without seasonal variations in temperature, i.e. noon-to-early afternoon hours during the hot season and/or evening/night hours during the cold period. Therefore, the analysis is limited to possible association with wind speed and direction.

The seasonal wind rose diagram is shown in Fig. 4 along with the seasonal distribution of N_{CN} (Fig. 5), N_{CCN} (Fig. 6) and AR (Fig. 7) at 0.31-0.33% S. The bivariate plots (Openair software; Carslaw and Ropkins, 2012) could help to better visualize and denote wind direction and air-mass origin (see section 3.4), while the colour in the plots represents the magnitude of wind speed, N_{CN}, N_{CCN} and AR. All year round, the winds were mostly from the northwest and southeast directions, with speed less than 5 m s^{-1}, indicating that the source of near-surface aerosols is related to local emissions and long-range transport, with the second mechanism dominating after examination of the diurnal patterns (Fig. 3). The southeasterlies clearly dominate during the monsoon and northwesterlies dominate during winter, while the two transition seasons have both wind directions (Fig. 4). The seasonally-changed wind directions significantly affect aerosol properties, N_{CCN} and N_{CN} due to long-range transported aerosols. The sensitivity of N_{CN} and N_{CCN} to wind direction is more pronounced in March, while it is lower during monsoon, suggesting that the rainy washout in this season reduces the influence of long-range aerosol transport over the GH region. N_{CN} (Fig. 5) seems to be larger from southern and southwestern directions during winter revealing the influence of IGP, while N_{CCN} (Fig. 6) follows a similar pattern in all seasons. In contrast, AR (Fig. 7) seems to be somewhat lower for southern directions during all seasons. This is more pronounced in winter, while in monsoon air masses from south could be associated with high AR values. Seasonal variations of N_{CCN}, N_{CN} and AR at 0.31-0.33% S in the four wind quadrants are summarized in Fig. 8, respectively. N_{CCN} and N_{CN} increase from monsoon toward pre-monsoon (March) in all four quadrants whereas AR increases from monsoon to post-monsoon and then remains almost constant for winter and March. The higher values of N_{CCN} and N_{CN} in 180^{o}-270^{o} and 270^{o}-360^{o} quadrants are due to the transport of aerosols from the IGP and west Asian regions, while the AR values are not strongly influenced by the wind direction. However, the sectors that are associated with high N_{CCN} and N_{CN} seem to have lower AR values, suggesting more hydrophobic aerosols.

3.4. Source analysis and long-range transport

In order to study aerosol source identification and the effects of long-range transport over the observation site, the 5-days isentropic air mass back trajectories at 500 m above ground level were analysed for 6 (00; 06; 12 and 18) hours singular. The HYSPLIT model (Draxler et al., 2012; http://ready.arl.noaa.gov/HYSPLIT.php) was used together with the Global Data Assimilation System (GDAS1) meteorological database as input to calculate the air mass back trajectories in each season (Fig. 9). The trajectories are colour-coded according

335 to the altitude attained by the air masses along the pathway before arriving at the observation
336 site.
337 During the winter season, the wind pattern over the observation site is mostly
338 northwesterly (Fig. 4a), while during the pre- and post-monsoon seasons the air masses
339 circulate around the observation site with a clear western preference during pre-monsoon.
340 The high values of N_{CN} and N_{CCN} during winter are due to the arrival of air masses from the
341 Indian subcontinent and Southwest Asia. It is interesting to note that the western air masses
342 travel at higher altitudes (above 3 km), lowering in height, usually below 1 km, while
343 approaching the observation site. The lower values of N_{CN} and N_{CCN} during the Indian
344 summer monsoon are mostly due to rainfall washout and not so much due to clean marine air
345 masses from the Bay of Bengal (Hyvärinen et al., 2011). The highest N_{CCN} and N_{CN} during
346 the pre-monsoon season (Fig. 8) are mostly associated with air-masses coming from the arid
347 west Asian countries (e.g. Pakistan, Afghanistan, Iran) and passing through the Thar Desert,
348 while during post-monsoon the contribution of biomass-burning aerosols from IGP increases
349 (Kaskaoutis et al., 2014). The analysis shows that the air masses are mostly within the
350 atmospheric boundary layer (<500-1000 m) near the observation site and progressively
351 increase in altitude at greater distances, either towards the west (winter/pre-monsoon) or
352 towards the east-southeast (monsoon). This suggests that boundary layer dynamics over the
353 polluted IGP play a prominent role in long-range transport and air mass uplift (Dumka et al.,
354 2014b).
355 The mixing-height was also obtained from the hourly intervals of the HYSPLIT
356 outputs and estimated using the Turbulent Kinetic Energy (TKE) profile method (Draxler et
357 al., 2012), in which the mixing height is assigned to the height at which TKE either decreases
358 by a factor of two or to a value less than 0.21 (m^2/s^2). The monthly statistics of the mixing
359 height at Nainital are given in Table 1 and the seasonal-mean diurnal variations are shown in
360 Fig. 10. The mixing height is lowest during December (271.5 ± 367.7 m ranging between
361 12.8 and 1043.6 m) and highest during June (672.6 ± 553.6 m ranging between 93.9 and
362 1546.9 m) following the thermal heating of the surface. Furthermore, its diurnal variation is
363 very strong, especially in March, with high values (~ 2000 m) during noon and just a few
364 meters during nighttime (Fig. 10). The diurnal pattern weakens in the other seasons; however,
365 it is characteristic of the boundary-layer dynamics trapping the aerosols near the ground
366 during the cold period of the year and during nighttime, and favouring their dilution (uplift to
367 higher altitudes) during noontime to afternoon. Opposite to that expected from the boundary-
368 layer dynamics, the diurnal variation of N_{CCN} and N_{CN} revealed higher values during noon-to-
369 early afternoon hours (Fig. 3) suggesting dominance of long-range transport of aerosols from
370 Ganges Basin and west Asia favoured in their uplift by the larger mixing height. In this
371 respect, Prabha et al. (2012) revealed the removal of pollution from the IGP to higher

atmospheric levels in association with dynamically forced updrafts. Their results showed that the valley pollution could be uplifted to heights above the haze layer, favoured by the buoyancy that is generated due to thermal heating of the surface during noon-to-early afternoon hours. It should be noted that the monthly-mean diurnal variations (Fig. 3), coincide well with the respective seasonal variations, thus allowing an association between variations in N_{CN}, N_{CCN} and boundary-layer height.

3.5. Relation of N_{CCN} with S

In this section, we examine the monthly-mean N_{CCN} as a function of S and determine the parameters for the "CCN spectrum" by following Jefferson (2010):

$$N_{CCN}(S) = cS^{k} \quad (1)$$

where S is the super-saturation in percent, c and k are constant terms that relate to the particle number concentration and chemical composition. Figure 11 shows the monthly and seasonal (winter and monsoon) means of N_{CCN} as a function of S, while the c and k parameters were estimated for different ranges of S (Table 3) using the least-square fit method in log-log scale (Khvorostyanov and Curry, 2006; Jefferson, 2010 and reference therein). The results show that the increasing trends of N_{CCN} with S are less steep during June to September (monsoon) compared to November - March (considered as winter), thus associated with lower k values. During monsoon, the variation of N_{CCN} is constant above S = 0.45%, suggesting no CCN with critical S (S_c) > 0.45%, whereas N_{CCN} increases from 1500 to 2500 during winter, suggesting more particles with S_c > 0.4%. The difference in increasing rates between the two seasons reveals differences in particle composition and size. The c and k values (0.10/0.17 – 0.75/0.78 S) range from 1092 ± 47 cm^{-3} (August) to 5065 ± 755 cm^{-3} (March) and 0.31 ± 0.13 (June) to 1.24 ± 0.12 (March), respectively (Table 3) and are, in general, within the range of values reported for continental aerosols (Seinfeld and Pandis, 1998), except for December to March, where the c values are higher suggesting more turbid atmospheres approaching urban conditions. The c value reflects the CCN concentration, while k shows the increase in CCN with S, which shows a decreasing tendency for increasing S (lower k values for larger S) (Hudson and Noble, 2014). This is mostly observed during the winter period, while during monsoon k does not present a clear tendency with S. The k values obtained at Nainital are higher than the value (k = 0.15) reported by Engelhart et al. (2008) for aged monoterpene secondary organic aerosols and Bhattu and Tripathi (2014) at Kanpur (0.16 ± 0.08) for dominance of organic species.

3.6. Correlation between N_{CCN} and N_{CN}

In this section, we further investigate the relationship between N_{CN} and N_{CCN} and AR. Figure 12 represent the scatter plots of N_{CCN} and AR as a function of N_{CN} (integrated at every 500 cm^{-3} bin) during the whole measurement period at three S, i.e. 0.31-0.33%, 0.46-0.48%

and 0.75-0.78 %. The vertical bars represent the standard deviations about the means, while the dotted lines are the fitted power-law functions [$Y = A(x-x_c)^P$ for N_{CCN} vs N_{CN} and $Y = a + bx^c$ for AR vs N_{CN}] for each S. The large standard deviations indicate that there is large variability in N_{CCN} for each N_{CN} interval, suggesting that it is difficult to estimate N_{CCN} over the GH region without having information about the chemical composition of aerosols (Yum et al., 2007). Figure 12a shows that for all S N_{CCN} increases with increasing N_{CN}, initially with a very high rate, which decrease above 5 – 6 x10^3 cm^{-3} N_{CN}. The AR shows decreasing trend with N_{CN}, which becomes greater as N_{CN} increases indicating that more turbid atmospheres are less CCN active. Similar results are also reported over Gosan, Korea for polluted air masses during the Atmospheric Brown Clouds-East Asian Regional Experiment (Yum et al., 2007).

Figure 13 presents the N_{CCN} variation as a function of N_{CN}, using raw data on seasonal basis at two S levels 0.31-0.33 (black color) and 0.75-0.78 (red color). Although the correlations appear to be similar in all seasons (i.e., increasing trend of N_{CCN} with N_{CN}), differences are observed in the respective regression slopes. Thus, during winter, pre-monsoon and monsoon, the regression slope between N_{CCN} and N_{CN} is about 0.37, while in post-monsoon it is higher (0.50) at 0.33% S, suggesting more CCN. At 0.75-0.78% S level, the slopes for post-monsoon, winter and pre-monsoon are similar (~0.63), while during monsoon the slope is much lower (0.45), resulting in small differences in AR between the two S levels. This indicates that N_{CCN} is either a weak (monsoon) or strong function of S. The results also reveal that the differences in N_{CCN} between the two S levels are much larger at high CN concentrations, suggesting that the larger aerosol loading needs higher S levels in order to be CCN. In contrast, for aerosol concentrations below ~ 3x10^3 cm^{-3}, N_{CN} is similar to N_{CCN} (especially in monsoon), revealing that the vast majority of particles are CCN.

In synopsis, the results revealed that the ratio of N_{CCN} to N_{CN} or AR is seasonally dependent over Nainital indicating influence of distinct aerosol sources, transport pathways, rainfall and mixing processes. Furthermore, the contrasting features of the N_{CN} vs N_{CCN} as a function of S for monsoon and winter are examined in Fig. 14(a-e). The correlation coefficients and the slopes of the linear regressions increase with the S levels for both seasons, but the activation of CN to CCN is more efficient in winter (larger slopes) than in monsoon (Fig. 14a-e). Furthermore, the slopes of activation increase in a faster rate with S level in winter (from 0.18 at 0.17% S to 0.63 for 0.77%S) compared to monsoon (from 0.21 at 0.17% S to 0.42 at 0.77% S), suggesting larger increase in AR as a function of S in winter (Fig. 14). Measurements at Puy-de-Dome (Asmi et al., 2012) revealed higher slope of CCN vs CN during winter (slope = 0.47 with R^2 = 0.80) than monsoon (slope = 0.13 with R^2 = 0.15), results that are similar to those found at Nainital.

3.7. Comparison between Nainital and IGP-Kanpur site

During the period June-August 2011, simultaneous measurements of N_{CCN} and N_{CN} were performed in Kanpur (independent from GVAX campaign). Figure 15a, b shows the daily variation of N_{CCN} and N_{CN}, respectively at Kanpur and Nainital (box and whisker chart view), while the daily-mean AR values are shown in Fig. 15c. For all the graphs the S level at Kanpur is 0.2% and at Nainital 0.17%. Considerable day-to-day variation is observed in the N_{CCN} and N_{CN} at both sites, which is much stronger in Kanpur due to higher rates of anthropogenic emissions that enhance the concentrations 3 to 4 times those observed at Nainital. The mean N_{CCN} at Kanpur was found to be 2408 ± 1030 cm^{-3} compared to 589 ± 288 cm^{-3} at Nainital, while the N_{CN} is 9862 ± 4694 cm^{-3} and 2132 ± 701 cm^{-3} at Kanpur and Nainital, respectively. On the other hand, on specific days (i.e. 24 June and 3 July, 2011) the CCN values at Kanpur and Nainital are comparable, but in the vast majority of the cases they exhibit significant differences in both N_{CCN} and N_{CN}. Besides large differences in the N_{CCN} and N_{CN}, the mean AR is comparable at both sites (0.30 ± 0.08 at Kanpur and 0.28 ± 0.15 at Nainital), in spite of the deviations that are observed on certain days due to different aerosol composition, the influence of various sources and additional anthropogenic emissions at Kanpur (Ram et al., 2008, 2010; Kumar et al., 2014). The consistency in the AR values suggests similarities in the origin, characteristics and chemical composition of aerosols, supporting transport from the Ganges valley to the Himalayan foothills. The differences between the two locations for higher S levels (0.31-0.4 and 0.75-0.8) were found to be similar to those at 0.2% S and the results are summarized in Table 4. Based on two years of continuous measurements of CCN and CN at Kanpur, Patidar et al. (2012) reported significant inter and intra-seasonal variations, which could be due to varying local emissions, influence of long-range transport and different chemical composition. In synopsis, the N_{CCN} and N_{CN} over Kanpur are very high (about 3-4 times more) compared to those at Nainital, attributed to the turbid environment over the Ganges basin during the whole year (Kaskaoutis et al., 2013).

4. Conclusions

The time-series analysis of N_{CN}, N_{CCN} and AR was presented in the framework of an intensive field campaign GVAX in the Gangetic - Himalayan region during June 2011 to March 2012. The measurements correspond to the Nainital site, located in Indian Himalayas (1958 m amsl) above the polluted Ganges basin. The main findings of the study are summarized as follows:

1. The CCN, CN and AR showed a pronounced monthly variation with high values during November to March and low during June to September.

2. Strong-to-neutral diurnal variation of N_{CCN} and N_{CN} was observed during the winter-to-summer season, with afternoon maximums, while the diurnal variation of AR was in opposite phase (morning maximum and noon minimum). The lower AR during noontime suggests more non-CCN particles transported from IGP. The diurnal cycles were attributed to the evolution of the atmospheric boundary layer and the uplift of pollutants from the IGP during the afternoon.
3. Seasonally-changing meteorological conditions favouring transport of aerosols from different sources, along with boundary-layer dynamics and RH variations, seem to play an important role in CCN concentrations. The air-mass back trajectories revealed dominance of aerosol transport from northwestern India and the west Asian regions, especially during winter and pre-monsoon. In contrast, during summer monsoon the air masses were mostly of marine origin and, combined with the rainy washout over northern India, they were associated with lower aerosol concentrations.
4. The average values of k obtained from the power law fit between N_{CCN} and S were found to range between 0.31 ± 0.13 (June) and 1.24 ± 0.12 (March), while k exhibited a decreasing trend with S during winter and was nearly constant in monsoon. Furthermore, the particles were found to have larger values of k during winter, whereas in monsoon N_{CCN} increases with S till ~0.45% S and remains rather constant above it. N_{CCN} increased significantly with increasing N_{CN}, but AR decreased with N_{CN} at all S levels suggesting that the more turbid atmospheres do not favour CCN.
5. The N_{CCN} and N_{CN} values at Nainital were much lower (3-4 times) than those measured at Kanpur during the monsoon period. In contrast, the mean AR was found to be similar at the two sites suggesting aerosols of similar origin and characteristics, although on some days it exhibited significant differences.

Acknowledgment

We acknowledge U.S. Department of Energy Atmospheric Radiation Measurements Climate Research Facility for providing database (http://www.archive.arm.gov/) for this work. This study is carried out under GVAX (https://www.arm.gov/sites/amf/pgh/) project in collaboration among the DoE, IISc, SPL, ISRO and ARIES. We would like to thank all the participants in the campaign (scientists and technicians) for their keen interest, data collection and kind support. HYSPLIT transport and dispersion model data (NOAA ARL) are used from READY website (http://www.arl.noaa.gov/ready.html) for the back-trajectory analysis. The authors are thankful to Dr N. Ojha and Dr David Carslaw for the fruitful discussion during the airmass back trajectory analysis. The authors are thankful to the referee for insightful comments and valuable suggestions, which helped us significantly in improving the scientific quality of the manuscript.

521 **References**

522 Andreae, M. O. and Rosenfeld, D., 2008. Aerosol-cloud-precipitation interactions Part 1, The
523 nature and sources of cloud-active aerosols. Earth-Sci. Rev., *89,* 13-41.
524 Andreae, M. O. et al., 2004. Smoking Rain Clouds over the Amazon. Science*,* 303*,* 1337-
525 1342.
526 Asmi, E., Freney E., Hervo M., Picard D., Rose C., Colomb A., and Sellegri K., 2012.
527 Aerosol cloud activation in summer and winter at puy-de-Dome high altitude site in
528 France Atmos. Chem. Phys., 12, 11589–11607, doi: 10.5194/acp-12-11589-2012.
529 Bhattu, D., and Tripathi, S.N., 2014. Inter-seasonal variability in size-resolved CCN
530 properties at Kanpur, India. Atmos. Environ., doi: 10.1016/j.atmosenv.2013.12.016.
531 Carslaw, D. C. and Ropkins, K. 2012. Openair-An R package for air quality data analysis.
532 Environ. Model. Softw., 27–28, 52–61.
533 Chakravarty, Mukhopadhyay` K., Taraphdar P. S. 2011. Cloud microphysical properties as
534 revealed by the CAIPEEX and satellite observations and evaluation of a cloud system
535 resolving model simulation of contrasting large scale environments. J. Atmos. Sol. Terr.
536 Phys., 73, 1790-1797.
537 Cheng, Y. F., Wiedensohler A., Eichler H. et al., 2008. Relative humidity dependence of
538 aerosol optical properties and direct radiative forcing in the surface boundary layer at
539 Xinken in Pearl River Delta of China: An observation based numerical study. Atmos.
540 Environ., 42(25), 6373-6397.
541 Dey S., and Di Girolamo L, 2010. A climatology of aerosol optical and microphysical
542 properties over the Indian Subcontinent from 9 years (2000-2008) of Multiangle Imaging
543 SpectroRadiometer (MISR) data. J. Geophys. Res., 115, D15204, doi:
544 10.1029/2009JD013395.
545 Dey, S., and Di Girolamo L., 2011. A decade of change in aerosol properties over the Indian
546 subcontinent. Geophys. Res. Lett., 38, L14811, doi: 10.1029/2011GL048153.
547 Dipu, S., Prabha Thara V., Pandithurai G., Dudhia J., Pfister G., Rajesh K., and Goswami
548 B.N. 2013. Impact of elevated aerosol layer on the cloud macrophysical properties prior
549 to monsoon onset. Atmos. Environ., 70, 454-467.
550 Draxler, R. et al., 2012., HYSPLIT4 user's guide, version 4, report, NOAA, Silver Spring,
551 Md. [www.arl.noaa.gov/documents/reports/hysplit_user_guide.pdf].
552 Dumka, U. C., and Kaskaoutis D. G., 2014. In-situ measurements of aerosol properties and
553 estimates of radiative forcing efficiency over Gangetic-Himalayan region during the
554 GVAX field campaign, Atmos. Environ., 94, 96-105.
555 Dumka, U. C., Krishna Moorthy K., Satheesh S. K., Sagar Ram and Pant P., 2008. Short
556 period modulations in aerosol optical depths over central Himalayas: Role of mesoscale
557 processes. J. Appl. Meteorol. Climatol, 47, 1467-1475.
558 Dumka U.C., Krishna Moorthy K., Kumar Rajesh, Hegde P., Sagar Ram, Pant P., Singh
559 Narendra and Babu S. Suresh 2010. Characteristics of aerosol black carbon mass
560 concentration over a high altitude location in the Central Himalayas from multi-year
561 measurements. Atmos. Res., 96, 510-521.
562 Dumka U.C., Krishna Moorthy K., Tripathi S. N., Hegde P. and Sagar Ram, 2011. Altitude
563 variation of aerosol properties over the Himalayan range inferred from spatial
564 measurements. J. Atmos. Sol-Terr. Phys., 73, 1747-1761.
565 Dumka U.C. Manchanda R. K., Sinha P. R., Sreenivasam S., Krishna Moorthy K. and Babu
566 S. Suresh, 2013. Temporal variability and radiative impact of black carbon aerosol over
567 tropical urban station Hyderabad. J. Atmos. Sol-Terr. Phys., 105-106, 81-90.
568 Dumka, U. C., Tripathi S. N., Misra A., Giles D. M., Eck T. F., Sagar R., and Holben B. N.,
569 2014a. Latitudinal variation of aerosol properties from Indo-Gangetic Plain to central

570 Himalayan foothills during TIGERZ campaign. J. Geophys. Res. Atmos., 119, doi:
571 10.1002/2013JD021040.
572 Dumka, U. C., Kaskaoutis D. G., Srivastava M. K., and Devara P. C. S., 2014b. Scattering
573 and absorption properties of near-surface aerosol over Gangetic-Himalayan region: the
574 role of boundary layer dynamics and long-range transport. Atmos. Chem. Phys. Discuss.,
575 14, 21101-21148, doi: 10.5194/acpd-14-21101-2014.
576 Dusek, U., Frank G.P., Hildebrandt L., Curtius J., Schneider J., Walter S., Chand D.,
577 Drewnick F., Hings Jung S., Borrmann D.S., Andreae M.O., 2006. Size matters more
578 than chemistry in controlling which particles can nucleate cloud droplets. Science, 312,
579 1375-1378.
580 Dutkiewicz, V., Sofia Alvi A., Ghauri Badar M., Choudhary M. Iqbal, Husain Liaquat, 2009.
581 Black carbon aerosols in urban air in South Asia, Atmos. Environ., 43, 1737-1744.
582 Elminir H. K., 2005. Dependence of urban air pollutants on meteorology. Sci. Total Environ,
583 350(1-3), 225-237.
584 Engelhart, G. J., Asa-Awuku A., Nenes A. and Pandis S. N., 2008., CCN activity and droplet
585 growth kinetics of fresh and aged monoterpene secondary organic aerosol. Atmos.
586 Chem. Phys., 8, 3937-3949.
587 Fitzgerald, J. W. (1973), Dependence of the supersaturation spectrum of CCN on aerosol size
588 distribution and composition, J. Atmos. Sci., 30, 628–634.
589 Friedman, B., Zelenyuk A., Beránek J., Kulkarni G., Pekour M., Hallar A. G., McCubbin I.
590 B., Thornton J. A., and Cziczo D. J., 2013. Aerosol measurements at a high elevation
591 site: composition, size, and cloud condensation nuclei activity. Atmos. Chem. Phys., 13,
592 11839–11851, doi: 10.5194/acp-13-11839-2013.
593 Gajananda, K., Kuniyal Jagdish C., Momin G.A., Rao P.S.P., Safai P.D., Tiwari S. and Ali
594 K., 2005. Trend of atmospheric aerosols over the north western Himalayan region, India.
595 Atmos. Environ., 39, 4817-4825.
596 Hitzenberger, R., Berner A., Giebl H., Kromp R., Larson S., Rouc A., Koch S.M., Puxbaum
597 H., 1999. Contribution of carbonaceous material to cloud condensation nuclei
598 concentrations in European background (Mt.Sonnblick) and urban (Vienna) aerosols.
599 Atmos. Env. 33, 2647–2659.
600 Hudson, J. G., and Yum S. S., 2002. Cloud condensation nuclei spectra and polluted and
601 clean clouds over the Indian Ocean. J. Geophys. Res., 107(D19), 8022, doi:
602 10.1029/2001JD000829.
603 Hudson, J.G., and Noble, S., 2014. CCN and vertical velocity influences on droplet
604 concentrations and supersaturations in clean and polluted stratus clouds. J. Atmos. Sci.,
605 71, 312-331.
606 Hyvärinen A. P., Raatikainen T., Komppula M., Mielonen T., Sundström A. M., Brus D.,
607 Panwar T. S., Hooda R. K., Sharma V. P., Leeuw G. de, and Lihavainen H., 2011. Effect
608 of the summer monsoon on aerosols at two measurement stations in Northern India-Part
609 2: Physical and optical properties. Atmos. Chem. Phys., 11, 8283-8294, doi:
610 10.5194/acp-11-8283-2011.
611 Jaidevi, J., Tripathi S. N., Gupta Tarun, Singh B. N., Gopalakrishnan V. and Dey Sagnik,
612 2011. Observation-based 3-D view of aerosol radiative properties over Indian
613 Continental Tropical Convergence Zone: Implications to regional climate. Tellus *B,*
614 *63(5), 971-989.*
615 Jefferson A., 2010. Empirical estimates of CCN from aerosol optical properties at four
616 remote sites. Atmos. Chem. Phys., 10, 6855–6861, doi: 10.5194/acp-10-6855-2010.

617 Jefferson, A., 2011. Aerosol Observing System (AOS) Handbook, U. S. Department of
618 Energy, DOE/SC- ARM/TR-014, available at
619 http://www.arm.gov/publications/tech_reports/handbooks/aos_handbook.pdf.
620 Jethva, H., Satheesh S. K., and Srinivasan J., 2005. Seasonal variability of aerosols over the
621 Indo-Gangetic basin. J. Geophys. Res., 110, D21204, doi: 10.1029/2005JD005938.
622 Junge, C.E., McLaren, E., 1971. Relationship of cloud nuclei spectra to aerosol size
623 distribution and composition. J. Atmos. Sci. 28, 382-390.
624 Jurănyi, Z, Gysel M., Weingartner E., DeCarlo P.F., Kammermann L., and Baltensperger U.,
625 2010. Measured and modelled cloud condensation nuclei number concentration at the
626 high alpine site Jungfraujoch. Atmos. Chem. Phys., 10, 7891–7906, doi: 10.5194/acp-10-
627 7891-2010.
628 Kaskaoutis D. G., Singh Ramesh P, Gautam Ritesh, Sharma Manish, Kosmopoulos P G and
629 Tripathi S N (2012), Variability and trends of aerosol properties over Kanpur, northern
630 India using AERONET data (2001-10). Environ. Res. Lett. 7, doi:10.1088/1748-
631 9326/7/2/024003.
632 Kaskaoutis, D.G., S. Kumar, D. Sharma, R.P. Singh, S.K. Kharol, M. Sharma, A.K. Singh, S.
633 Singh, A. Singh, D. Singh, 2014. Effects of crop residue burning on aerosol properties,
634 plume characteristics and long-range transport over northern India. J. Geophys. Res., (in
635 press), doi: 10.1002/2013JD021357
636 Kaskaoutis, D.G., Sinha P.R., Vinoj V., Kosmopoulos P.G., Tripathi S.N., Misra Amit,
637 Sharma M., Singh R.P., 2013. Aerosol properties and radiative forcing over Kanpur
638 during severe aerosol loading conditions. Atmos. Environ., 79, 7-19.
639 Kaufman, Y. J., Tanre, D., and Boucher, O., 2002. A satellite view of aerosols in the climate
640 system. Nature, 419, 215–223, doi: 10.1038/nature01091.
641 Khvorostyanov, V. I., and Curry J. A., 2006. Aerosol size spectra and CCN activity spectra:
642 Reconciling the lognormal, algebraic, and power laws. J. Geophys. Res., 111, D12202,
643 doi: 10.1029/2005JD006532.
644 Kleissl, J. Honrath, R. E., Dziobak M. P., Tanner D., Martin M. Val, Owen R. C., and Helmig
645 D., 2007. Occurrence of upslope flows at the Pico mountaintop observatory: A case
646 study of orographic flows on a small, volcanic island. J. Geophys Res, 112, D10S35, doi:
647 10.1029/2006JD007565.
648 Komppula, M., Lihavainen H., Hyvärinen A. P., Kerminen V. M., Panwar T. S., Sharma V.
649 P., and Viisanen Y., 2009. Physical properties of aerosol particles at a Himalayan
650 background site in India. J. Geophys. Res., 114, D12202, doi: 10.1029/2008JD011007.
651 Konwar, M., Maheskumar R. S., Kulkarni J. R., Freud E., Goswami B. N., and Rosenfeld D.,
652 2012. Aerosol control on depth of warm rain in convective clouds. J. Geophys. Res., 117,
653 D13204, doi: 10.1029/2012JD017585.
654 Kumar, R., Barth M.C., Pfister G.G., Naja M., and Brasseur G.P., 2014. WRF-Chem
655 simulations of a typical pre-monsoon dust storm in northern India: influences on aerosol
656 optical properties and radiation budget. Atmos. Chem. Phys., 14, 2431–2446.
657 Lance, S., Medina, J., Smith, J. N., and Nenes, A., 2006. Mapping the Operation of the DMT
658 Continuous Flow CCN Counter. Atmos. Sci. Tech., 40, 242-254.
659 Lance, S., Nenes, A., Claudio, M., Dubey, M.K., Gates, H., Varutbangkul, V., Rissman, T.A.,
660 Murphy, S.M., Sorooshian, A., Flagan, R.C., Seinfeld, J.H., Feingold, G., Jonsson, H. H.,
661 2009. Cloud condensation nuclei activity, closure, and droplet growth kinetics of
662 Houston aerosol during the Gulf of Mexico Atmospheric Composition and Climate
663 Study (GoMACCS). J. Geophys. Res. 114, D00F15, doi: 10.1029/2008JD011699.

664 Lathem, T.L., Nenes, A., 2011. Water vapor depletion in the DMT continuous-flow CCN
665 chamber: effects on supersaturation and droplet growth. Aerosol Sci. Technol. 45, 604-
666 615.
667 Lawrence, M. G., 2011. Atmospheric science: Asia under a high-level brown cloud. Nat.
668 Geosci, 4, 30 352-353.
669 Lawrence, M. G., and Lelieveld J., 2010. Atmospheric pollutant outflow from southern Asia:
670 A review. Atmos. Chem. Phys., 10, 11017-11096.
671 Lee, S., Ghim Y. S., Kim S.W., Yoon S.C., 2010. Effect of biomass burning and regional
672 background aerosols on CCN activity derived from airborne in-situ measurements,
673 Atmos. Env. 44, 5227-5236.
674 Liu, J., Zheng Y., Li Z., and Cribb M., 2011. Analysis of cloud condensation nuclei
675 properties at a polluted site in southeastern China during the AMF-China Campaign. J.
676 Geophys. Res., 116, D00K35, doi: 10.1029/2011JD016395.
677 Lohmann, U., and Feichter, J., 2005, Global Indirect Aerosol Effects: A Review. Atmos.
678 Chem. Phys., 5,715-737.
679 Lu, Z, Zhang Q., and Streets D.G., 2011. Sulfur dioxide and primary carbonaceous aerosol
680 emissions in China and India, 1996–2010. Atmos. Chem. Phys., 11, 9839-9864
681 Manoharan V. S, Kotamarthi R., Feng Y., and Cadeddu M. P., 2014. Increased absorption by
682 coarse aerosol particles over the Gangetic–Himalayan region. Atmos. Chem. Phys., 14,
683 1159–1165.
684 Moorthy, K. K., Sreekanth V., Chaubey Jai Prakash Gogoi Mukunda M., Babu S. Suresh,
685 Kompalli Sobhan Kumar, Bagare S. P., Bhatt Bhuvan C., Gaur Vinod K., Prabhu T. P.,
686 and Singh N. S., 2011. Fine and ultrafine particles at a near–free tropospheric
687 environment over the high-altitude station Hanle in the Trans-Himalaya: New particle
688 formation and size distribution. J. Geophys. Res., 116, D20212, doi:
689 10.1029/2011JD016343.
690 Nishita, C., Osada K., Matsunaga K., and Iwasaka Y., 2007. Number-size distributions of
691 free tropospheric aerosol particles at Mt. Norikura, Japan: Effects of precipitation and air
692 mass transportation pathways. J. Geophys. Res., 112, D10213, doi:
693 10.1029/2006JD007969.
694 Padmakumari, B., Maheskumar R. S, Harikishan G., Morwal S. B., Prabha T. V., Kulkarni J.
695 R., 2013. In situ measurements of aerosol vertical and spatial distributions over
696 continental India during the major drought year 2009. Atmos. Environ., 80, 107-121.
697 Panday, A. K. and Prinn, R. G., 2009. Diurnal Cycle of air pollution in the Kathmandu
698 Valley, Nepal: Observations. J. Geophys. Res., 114, D09305, doi:
699 10.1029/2008JD009777.
700 Panday, A. K., Prinn, R. G., and Schär, C., 2009. Diurnal cycle of air pollution in the
701 Kathmandu Valley, Nepal: 2. Modeling results. J. Geophys. Res., 114, D21308, doi:
702 10.1029/2008JD009808.
703 Patidar V., Tripathi S. N., Bharti P. K., and Gupta T., 2012., First Surface Measurement of
704 Cloud Condensation Nuclei over Kanpur, IGP: Role of Long Range Transport. Aeros.
705 Sci. Tech., 46, 973-982.
706 Prabha T.V., Karipot A., Axisa D., Padmakumari B., Maheskumar R. S., Konwar M.,
707 Kulkarni J. R., and Goswami B. N., 2012, Scale interactions near the foothills of
708 Himalaya during CAIPEEX. J. Geophys. Res., 117, D10203, 495 doi:
709 10.1029/2011JD0167.
710 Pruppacher, H. R. and Klett J. D., 1997. Microphysics of clouds and precipitation. Kluwer
711 Academic Publishers, Dordrecht, 288-289.

712 Raatikainen T., Hyvärinen A.-P., Hatakka J., T. Panwar S., Hooda R. K., Sharma V. P.,
713 Lihavainen H., 2014. The effect of boundary layer dynamics on aerosol properties at the
714 Indo-Gangetic plains and at the foothills of the Himalayas, Atmos. Environ. 89, 548-555,
715 http://dx.doi.org/10.1016/j.atmosenv.2014.02.058.
716 Ram Kirpa, Sarin M.M., Hegde P., 2008. Atmospheric abundances of primary and secondary
717 carbonaceous species at two high-altitude sites in India: Sources and temporal
718 variability. Atmos. Environ., 42, 6785–6796.
719 Ram Kirpa, Sarin M.M., Tripathi S.N., 2010. A 1 year record of carbonaceous aerosols from
720 an urban site in the Indo-Gangetic Plain: Characterization, sources, and temporal
721 variability. J. Geophys. Res., 115, D24313, doi: 10.1029/2010JD014188.
722 Ram Kirpa, Tripathi S. N., Sarin M. M. and Bhattu D. 2014. Primary and secondary aerosols
723 from an urban site (Kanpur) in the Indo-Gangetic Plain: Impact on CCN, CN
724 concentrations and optical properties. Atmos. Environ., 89 (2014) 655-663.
725 Ramanathan, V., Crutzen P. J., Kiehl J. T., Rosenfeld D., 2001. Aerosols, Climate and
726 Hydrological Cycle. Science, 294, 2119-2124.
727 Robert, G. C., and Nenes, A., 2005. A Continuous Flow Streamwise Thermal gradient CCN
728 Chamber for Atmospheric Measurements. Aeros. Sci. Tech., 39, 206-221.
729 Rose, D, S.S., Gunthe, Mikhailov E Frank, GP, U., Dusek, M.O., Andreae, U., Poschl, 2008.
730 "Calibration and measurement uncertainties of continuous-flow cloud condensation
731 nuclei counter (DMT-CCNC): CCN activation of ammonium sulfate and sodium
732 chloride aerosol particles in theory and experiment." Atmos. Chem. Phys., 8, 1153–1179.
733 Rosenfeld, D., Lohmann Ulrike, Raga Graciela B., O'Dowd Colin D., Kulmala Markku,
734 Fuzzi Sandro , Reissell Anni , Andreae Meinrat O., 2008. Flood or Drought: How do
735 Aerosols Affect Precipitation?. Science, 321, 1309.
736 Sarangi T., Naja Manish, Ojha N., Kumar R., Lal S., Venkataramani S., Kumar A., Sagar R.
737 and Chandola H. C., 2014. First simultaneous measurements of ozone, CO and NO_y at a
738 high altitude regional representative site in the central Himalayas. J. Geophys. Res., doi:
739 10.1002/2013JD020631.
740 Seinfeld, J. H. and Pandis, S. N., 1998. Atmospheric Chemistry and Physics: From Air
741 Pollution to Climate Change. A Wiley Interscience Publication, USA, 1998.
742 Sellegri, K. P. Laj, H. Venzac, J. Boulon, D. Picard, P. Villani, P. Bonasoni, A. Marinoni, P.
743 Cristofanelli, and E. Vuillermoz et al., 2010. Seasonal variations of aerosol size
744 distributions based on long-term measurements at the high altitude Himalayan site of
745 Nepal Climate Observatory-Pyramid (5079 m), Nepal. Atmos. Chem. Phys., 10, 10679-
746 10690.
747 Shrestha P. Barros A. P., and Khlystov A., 2010. Chemical composition and aerosol size
748 distribution of the middle mountain range in the Nepal Himalayas during the 2009 pre-
749 monsoon season. Atmos. Chem. Phys., 10, 11605-11621.
750 Shrestha, P., Barros Ana P., Khlystov Andrei, 2013. CCN estimates from bulk hygroscopic
751 growth factors of ambient aerosols during the pre-monsoon season over Central Nepal.
752 Atmos. Environ., 67, 120-129.
753 Srivastava A. K., Tiwari S., Devara P. C. S., Bisht D. S., Srivastava Manoj K., Tripathi S. N.,
754 Goloub P., and Holben B. N., 2011. Pre-monsoon aerosol characteristics over the Indo-
755 Gangetic Basin: Implications to climate impact. Ann. Geophys., 29, 789-804.
756 Srivastava Monika, Tripathi S. N., Dwivedi A. K., Dalai Rosalin, Bhattu Deepika, Bharti P.
757 K., Jaidevi J. and Gupta Tarun, 2013. CCN closure results from Indian Continental
758 Tropical Convergence Zone (CTCZ) aircraft experiment. Atmos. Res., 132-133, 322-
759 331.

760 Tripathi, S. N., Dey Sagnik, Tare Vinod, Satheesh S. K., Lal Shyam and Venkataramani S.,
761 2005. Enhanced layer of black carbon in a north Indian industrial city. Geophys. Res.
762 Lett., 32, L12802, doi: .1029/2005GL022564.
763 Twomey, S., 1977. The Influence of Pollution on the Shortwave Albedo of Clouds. J. Atmos.
764 Sci., 34, 1149-1152.
765 Venzac, H., Sellegri K., Villani P., Picard D., and Laj P., 2009. Seasonal variation of aerosol
766 size distributions in the free troposphere and residual layer at the puy de Dome station,
767 France. Atmos. Chem. Phys., 9, 1465–1478.
768 Yum, S. S., Hudson J. G., Song K. Y. and Choi B. C., 2005. Springtime cloud condensation
769 nuclei concentrations on the west coast of Korea. Geophys. Res. Lett., 32, L09814, doi:
770 10.1029/2005GL022641.
771 Yum, S. S., Roberts G., Kim J. H., Song K., and Kim D., 2007. Submicron aerosol size
772 distributions and cloud condensation nuclei concentrations measured at Gosan, Korea,
773 during the Atmospheric Brown Clouds–East Asian Regional Experiment 2005. J.
774 Geophys. Res., 112, D22S32, doi: 10.1029/2006JD008212.

775 **Table 1:** Monthly statistics of CCN, CN and AR for S = 0.31 - 0.33% and mixing height derived from HYSPLIT.

Month	N_{CCN} (cm^{-3})				N_{CN}(cm^{-3})				AR =N_{CCN}/N_{CN}				Mixing Height (in meter)			
	Mean ± SD	Min	Med	Max	Mean ±SD	Min	Med	Max	Mean ± SD	Min	Med	Max	Mean ± SD	Min	Med	Max
Jun	925 ± 601	77	911	2454	2425 ± 1112	785	2420	4955	0.38 ± 0.11	0.11	0.40	0.56	672.62 ± 553.56	93.86	543.01	1546.92
Jul	881 ± 500	257	733	2738	1874 ± 776	1062	1693	4951	0.47 ± 0.11	0.20	0.50	0.65	464.60 ± 364.61	91.52	373.61	1039.49
Aug	684± 396	24	760	1400	1606 ± 453	702	1662	2427	0.42 ± 0.18	0.03	0.48	0.67	381.85 ± 366.40	64.29	296.46	866.44
Sep	1233 ± 677	351	1045	2763	2304 ± 904	1323	1978	4577	0.54 ± 0.12	0.23	0.58	0.72	371.16 ± 366.40	25.26	214.90	1008.40
Nov	2026 ± 813	739	1914	3649	3485 ± 1062	1954	3460	6555	0.60 ± 0.12	0.33	0.62	0.77	314.38 ± 387.78	13.83	20.76	1066.31
Dec	1465 ± 510	670	1440	2574	3193 ± 1065	1332	3184	5808	0.52 ± 0.11	0.16	0.54	0.69	271.52 ± 367.71	12.82	16.32	1043.61
Jan	1500 ± 591	144	1463	2739	3155 ± 934	876	3183	5648	0.49 ± 0.10	0.20	0.52	0.65	365.11 ± 469.32	35.39	56.33	1402.45
Feb	1757 ± 397	880	1718	2531	3383 ± 708	1698	3308	4844	0.54 ± 0.06	0.41	0.55	0.64	401.31 ± 497.93	37.81	93.81	1490.72
Mar	2065 ± 476	1253	1985	3247	4124 ± 747	2708	3944	5835	0.54 ± 0.09	0.40	0.52	0.74	548.36 ± 638.77	25.79	211.21	1921.10

776

777 **Table 2:** Comparison of N_{CN}, N_{CCN} and AR over Nainital during GVAX campaign along with those measured at high altitude sites.

Site Name (Altitude)	Sampling Period	N_{CCN} (cm^{-3}) Mean ± SD	N_{CN} (cm^{-3}) Mean ± SD	AR Mean ± SD	References
Nainital (~1958m amsl)	Jun 2011-Mar 2012 Monsoon (JJA) Winter (DJF)	1264 ± 895 836 ± 618 1590 ± 892	2619 ± 1738 1955 ± 1271 3211 ± 1801	0.49 ± 0.19 at 0.31-0.33% S 0.42 ± 0.20 at 0.31-0.33% S 0.52 ± 0.17 at 0.31 -0.33% S	Present Study
Puy-de-Dome (1465 m), France	Jun–Jul 2011 (Summer) Jan-Feb 2012 (Winter)	200-2000 50-3000	100 -10000	0.2 – 0.7 at 0.24% S	Asmi et al., 2012
Mt Sonnblick (3104 m), Austria	September 1995 July 1996	80-570 (mean=243) at 0.5% S 29-786 (mean=402) at 0.5% S			Hitzenberger et al., 1999
Storm Peak Laboratory (3210m), Northwestern Colorado	March 2011	1-470	400-2000		Friedman et al., 2013
Jungfraujoch (3580 m), Switzerland	May 2008	0.1-600 (149 ± 171) at 0.12% S 27-1582 (568±401) at 1.18% S	40-1720 (550)		Jurănyi et al, 2010

778

779

Table 3: Monthly mean values of c and *k* parameters at Nainital obtained from the power law fit (Eq. 1) for different S ranges.

Month	*c*	*k*	*k* (0.17-0.31)	*k* (0.31-0.46)	*k* (0.46-0.60)	*k* (0.60 - 0.75)
	S range (0.17, 0.31, 0.46, 0.60 & 0.75)					
Jun	1708 ± 256	0.57 ± 0.11	0.619	0.652	0.663	0.569
Jul	1386 ± 97	0.45 ± 0.08	0.615	0.652	0.651	0.561
Aug	1092 ± 47	0.45 ± 0.04	0.623	0.649	0.650	0.556
Sep	1607 ± 61	0.39 ± 0.03	0.632	0.655	0.648	0.554
	S range (0.10, 0.22, 0.33, 0.48, 0.63 & 0.78)		***k* (0.22-0.33)**	***k* (0.33-0.48)**	***k* (0.48-0.63)**	***k* (0.63 - 0.78)**
Nov	3005 ± 233	0.73 ± 0.06	0.704	0.645	0.617	0.531
Dec	3123 ± 514	1.13 ± 0.13	0.666	0.633	0.623	0.533
Jan	3678 ± 328	0.87 ± 0.11	0.680	0.643	0.624	0.533
Feb	3523 ± 545	1.06 ± 0.15	0.667	0.645	0.624	0.533
Mar	5065 ± 755	1.24 ± 0.12	0.669	0.637	0.615	0.531

Table 4: Mean (± SD) values of N_{CCN}, N_{CN} and AR at Kanpur and Nainital during June to August 2011.

	Kanpur			Nainital		
	S = 0.2%	S = 0.4%	S = 0.8%	S = 0.17%	S = 0.31%	S = 0.75%
N_{CCN}	2408 ± 1030	3682 ± 1093	3868 ± 944	589 ± 288	927 ± 397	1265 ± 499
N_{CN}	9862 ± 4694	9862 ± 4694	9862 ± 4694	2132 ± 701	2118 ± 665	2078 ± 665
AR	0.30 ± 0.08	0.48 ± 0.10	0.70 ± 0.24	0.28 ± 0.15	0.42 ± 0.14	0.47 ± 0.17

Seasonal inhomogeneity in cloud precursors over Gangetic Himalayan region during GVAX campaign

U. C. Dumka[1], Deepika Bhattu[2], S. N. Tripathi[2], D. G. Kaskaoutis[3], and B. L. Madhavan[4]*

[1]*Aryabhatta Research Institute of observational sciences (ARIES), Nainital, India*

[2]*Department of Civil Engineering, Indian Institute of Technology, Kanpur, India*

[3]*Department of Physics, School of Natural Sciences, Shiv Nadar University, India*

[4]*Leibniz Institute for Tropospheric Research (TROPOS), Germany*

[E-mail: dumka@aries.res.in; dimitris.kaskaoutis@snu.edu.in; snt@iitk.ac.in]

Figure Captions:

Figure 1:- Topography map with measuring sites referred in the text.

Figure 2:- Temporal variation of cloud condensation nuclei (N_{CCN}), condensation nuclei (N_{CN}) and activation ratio (AR) at four (0.17-0.22%, 0.31-0.33%, 0.46-0.48% and 0.75-0.78%, respectively) S levels during June 2011 to March 2012.

Figure 3:- Monthly-mean diurnal variation of N_{CCN}, N_{CN} and AR at 0.31-0.33% S during June, November, December and March. The vertical bars correspond to one standard deviation.

Figure 4:- Wind-rose diagram during monsoon (June - August), post-monsoon/autumn (September - November), winter (December - February) and pre-monsoon/spring (March only) based on measurements taken from June 2011 to March 2012. The grey circles show the % frequencies of counts per wind direction.

Figure 5:- Wind dependency of N_{CN} (cm^{-3}) at 0.31- 0.33% S.

Figure 6:- Same as in Fig. 5, but for N_{CCN}.

Figure 7:- Same as in Fig. 5, but for AR.

Figure 8:- Seasonal-mean variation of N_{CCN}, N_{CN} and AR (% in 4 quadrants: 0^o-90^o, 90^o-180^o, 180^o-270^o and 270^o-360^o, respectively) at 0.31-0.33% S. The vertical bars correspond to one standard deviation.

Figure 9:- Five-day HYSPLIT air mass back trajectories end at 500 m AGL at Nainital for the four seasons. The colour scale represents the travelling altitude by the air mass before reaching at the observation site.

Figure 10:- Seasonal-mean diurnal variation of the mixing height (MH) over Nainital in box and whisker charts view. Box represents the 50% (from 25-75%) of the values. Horizontal lines inside box represent mean (thin line) and median (thick line), respectively.

Figure 11:- (a) Monthly-averaged N_{CCN} as a function of S and, (b) N_{CCN} variation as a function of S for winter (December – February) and monsoon (June – August).

Figure 12:- (a) N_{CCN} and (b) AR at different S (0.31-0.33%, 0.46-0.48% and 0.75-0.78%, respectively) levels as a function of N_{CN}, which is integrated over 500/cm^3 bins. The vertical bars represent the standard deviation. The power law fits are shown as dotted lines.

Figure 13: Correlation between N_{CN} and N_{CCN} at two S levels 0.31-0.33 (black color) and 0.75-0.78 (red color) in each season at Nainital. The whole set of measurements was used in the correlations, while the slope and R^2 values of the linear regressions are given for each case.

Figure 14: Scatter plot between N_{CN} and N_{CCN} at five S levels during winter (December-January; red color) and monsoon (June-August; black color). The dash and solid lines shows the linear least square fits between N_{CN} and N_{CCN}. The slope and R^2 values of the linear regressions are also given in each panel.

Figure 15:- Daily average values of N_{CCN} (a), N_{CN} (b) and AR (c) in Kanpur and Nainital during June to August 2011. For all the graphs the S level at Kanpur is 0.2% and at Nainital 0.17%. The boxes correspond to 50% (25-75%) of the values and the vertical bars correspond to one standard deviation. The solid lines into the boxes stand for the mean.

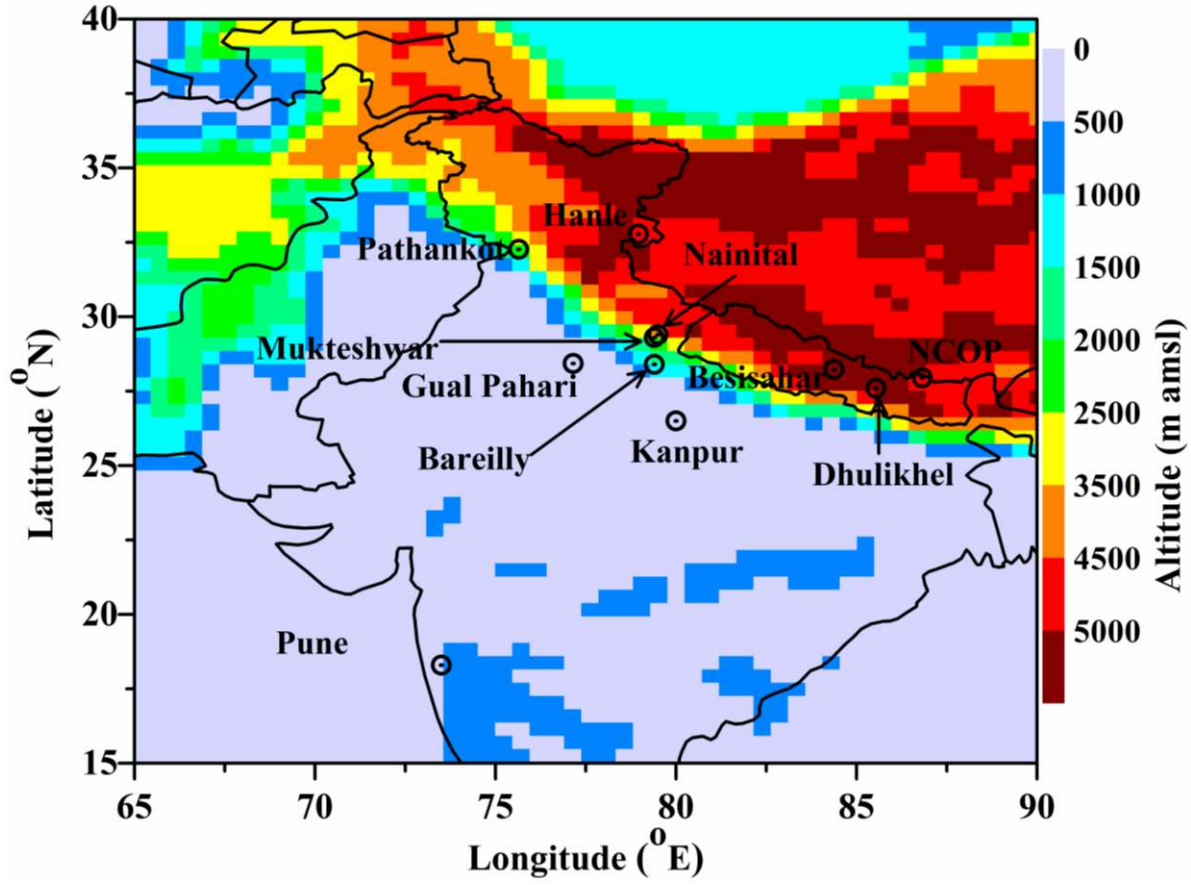

Figure 1

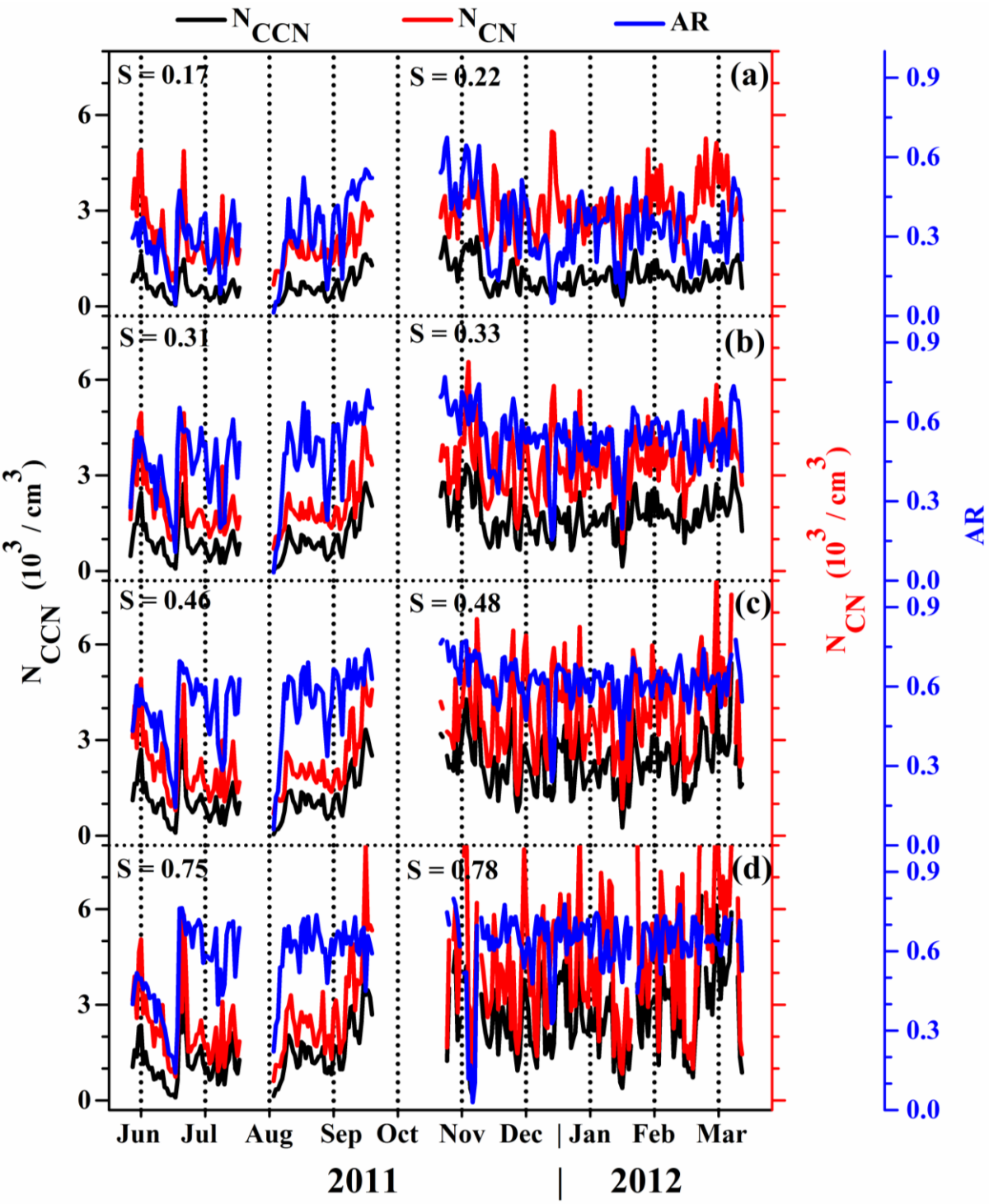
N_CCN
N_CN
AR
S = 0.17
S = 0.22
(a)
S = 0.31
S = 0.33
(b)
S = 0.46
S = 0.48
(c)
S = 0.75
S = 0.78
(d)
N_CCN (10^3 / cm^3)
N_CN (10^3 / cm^3)
AR
Jun Jul Aug Sep Oct Nov Dec | Jan Feb Mar
2011 | 2012

Figure 2

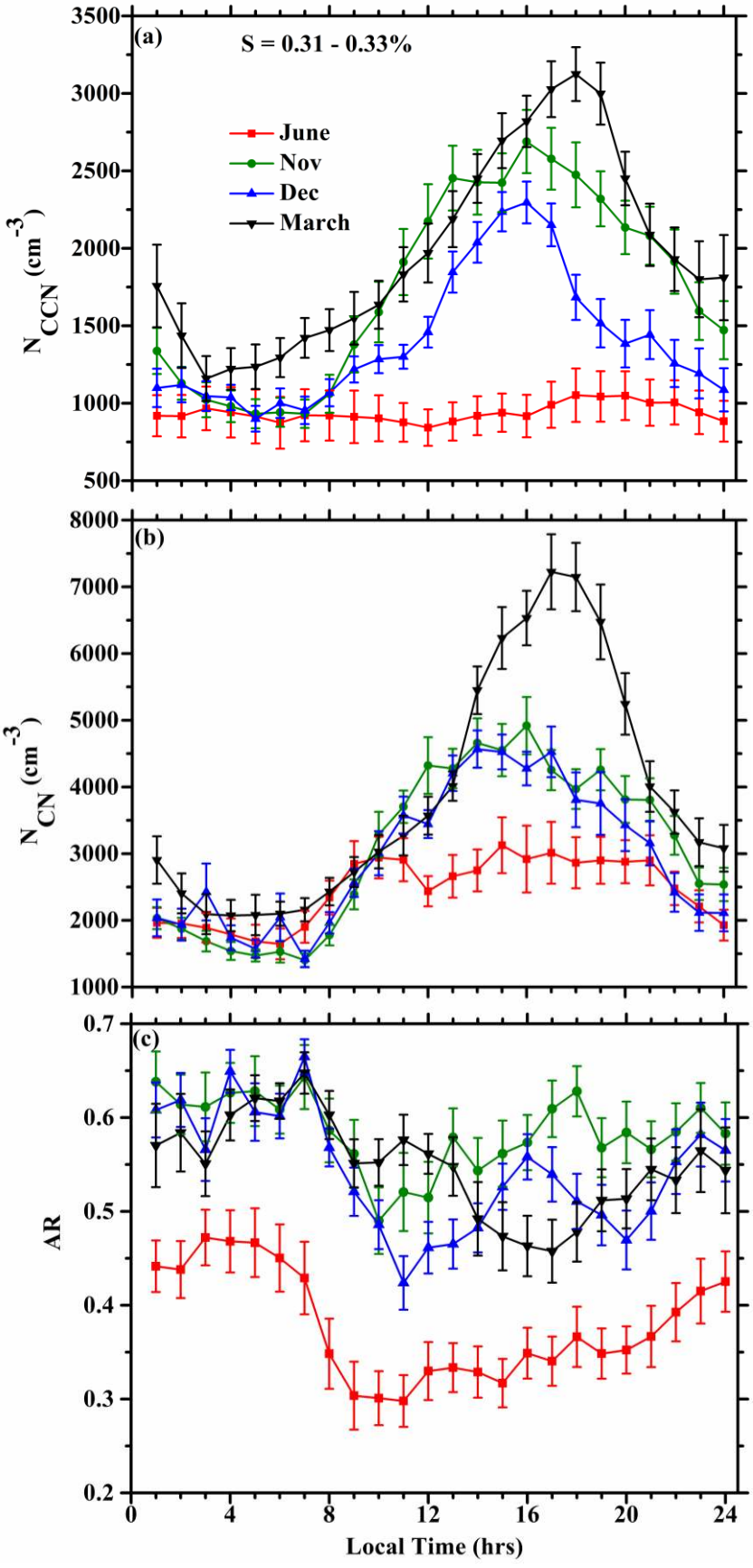
(a)
S = 0.31 - 0.33%
June
Nov
Dec
March
N_{CCN} (cm^{-3})
(b)
N_{CN} (cm^{-3})
(c)
AR
Local Time (hrs)

Figure 3

63

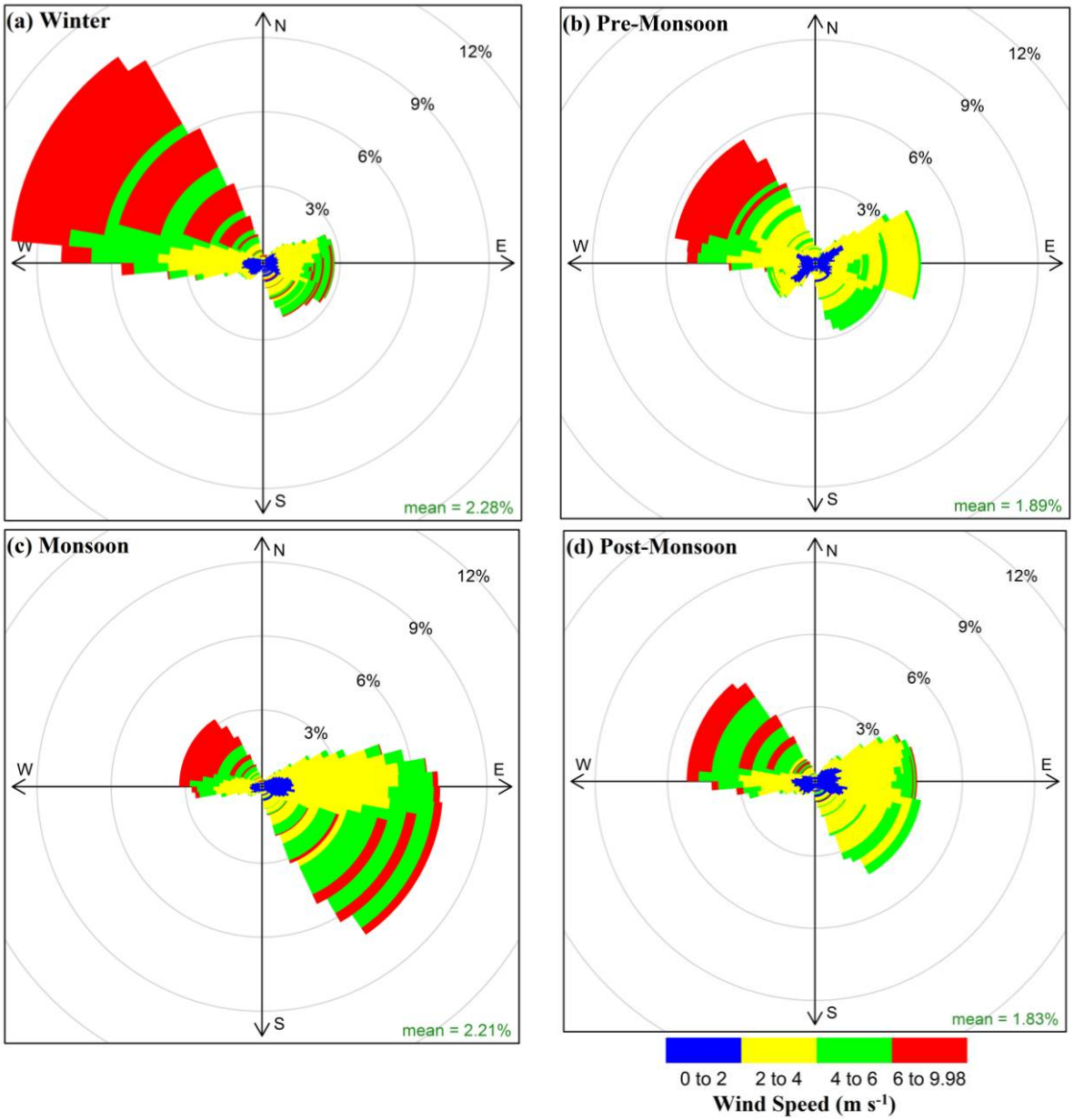

64 **Figure 4**

65

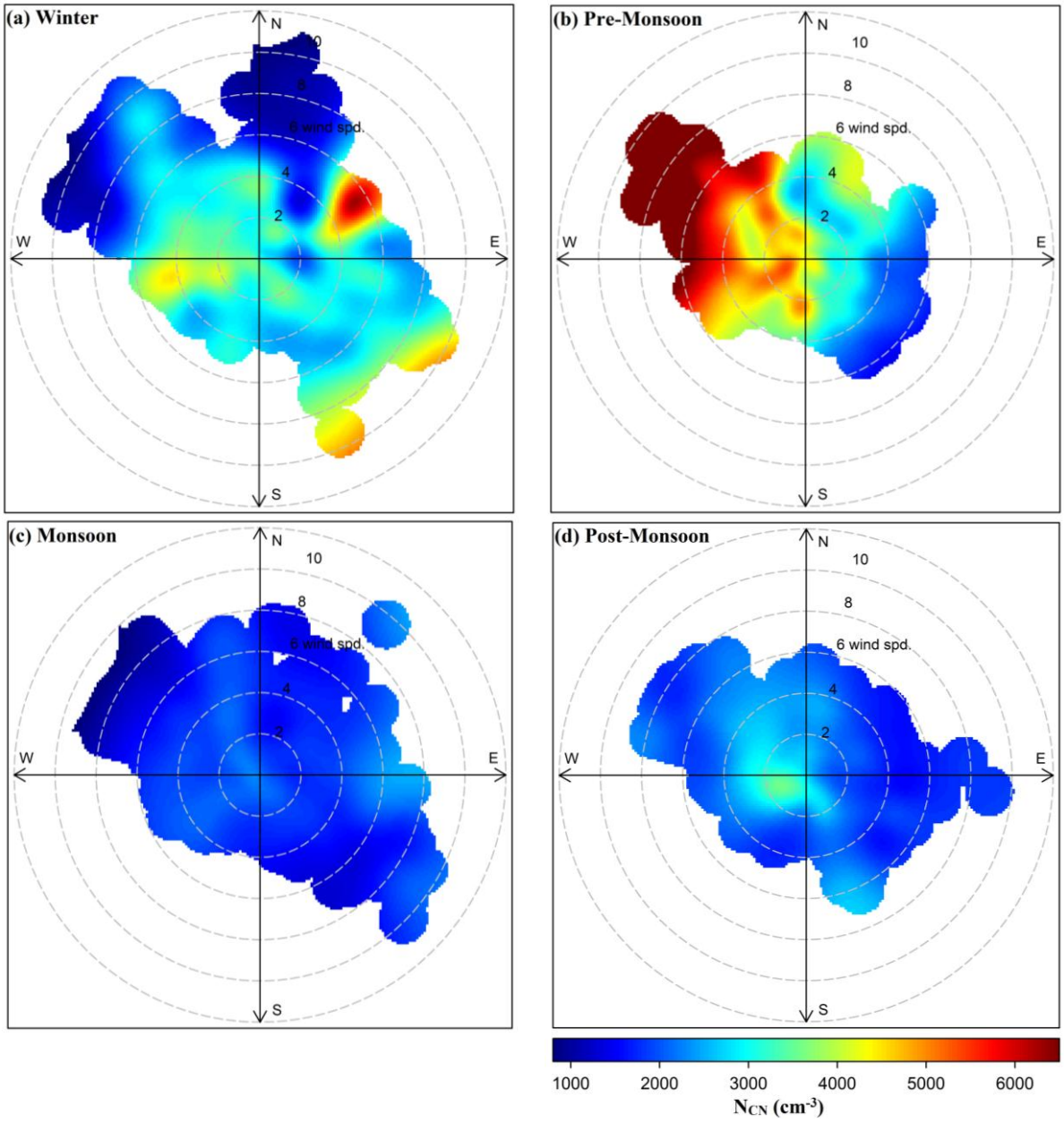
(a) Winter
(b) Pre-Monsoon
(c) Monsoon
(d) Post-Monsoon
N
S
W
E
10
8
6 wind spd.
4
2
1000
2000
3000
4000
5000
6000
N_{CN} (cm^{-3})

Figure 5

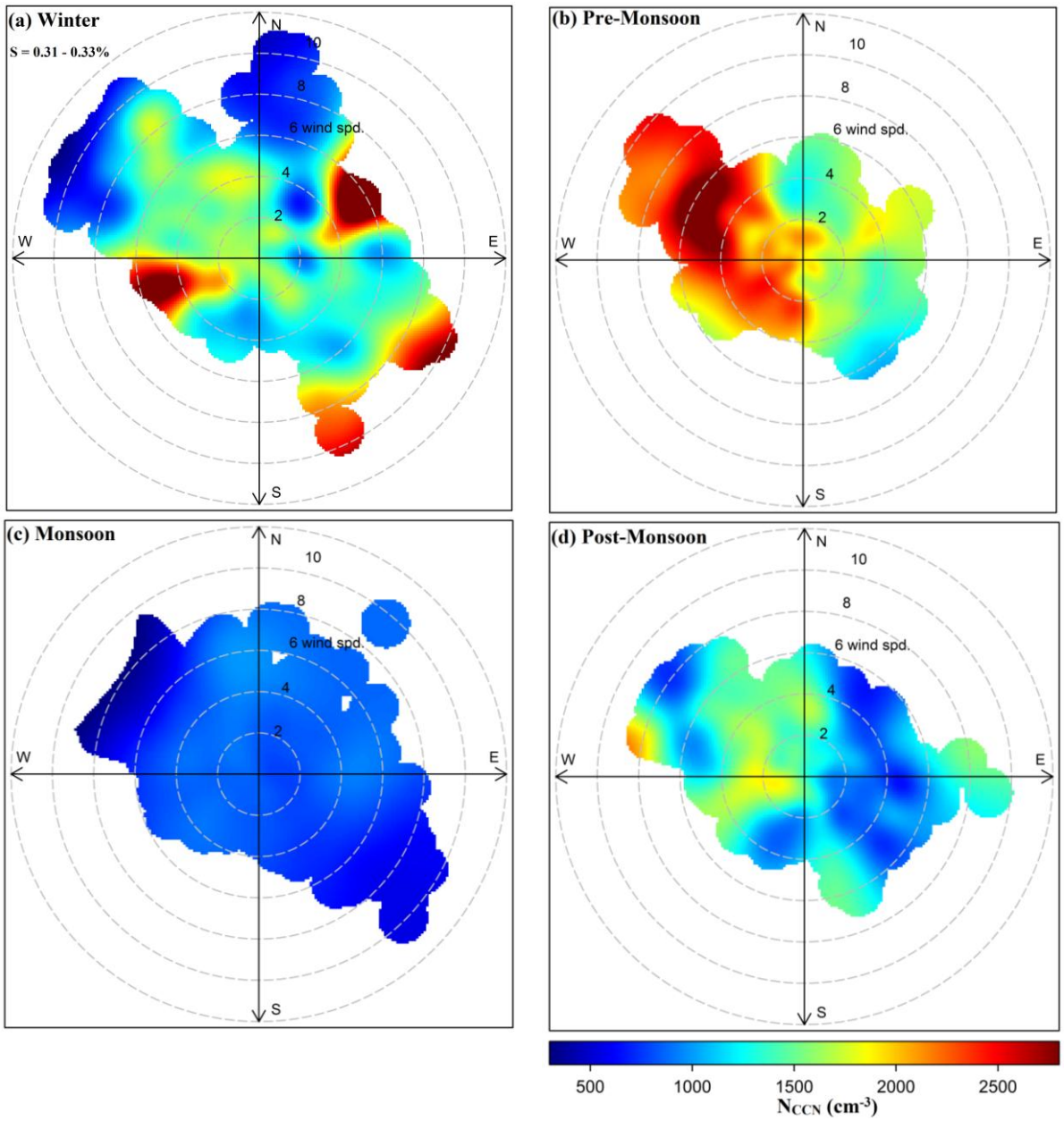
(a) Winter
S = 0.31 - 0.33%
(b) Pre-Monsoon
(c) Monsoon
(d) Post-Monsoon
N
S
W
E
10
8
6 wind spd.
4
2
500
1000
1500
2000
2500
NCCN (cm-3)

Figure 6

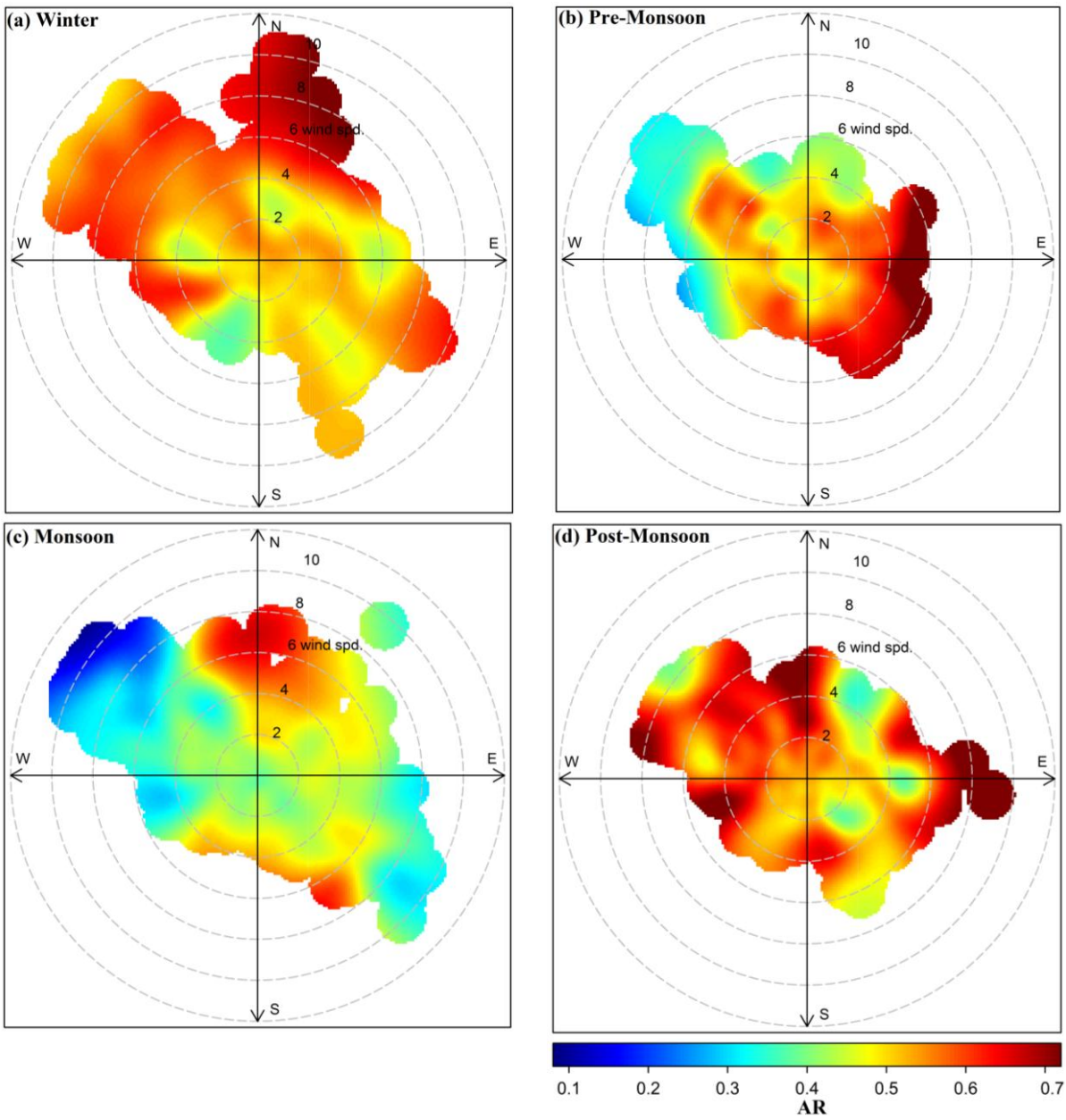
(a) Winter
(b) Pre-Monsoon
(c) Monsoon
(d) Post-Monsoon
N
S
W
E
2
4
6 wind spd.
8
10
0.1
0.2
0.3
0.4
0.5
0.6
0.7
AR

Figure 7

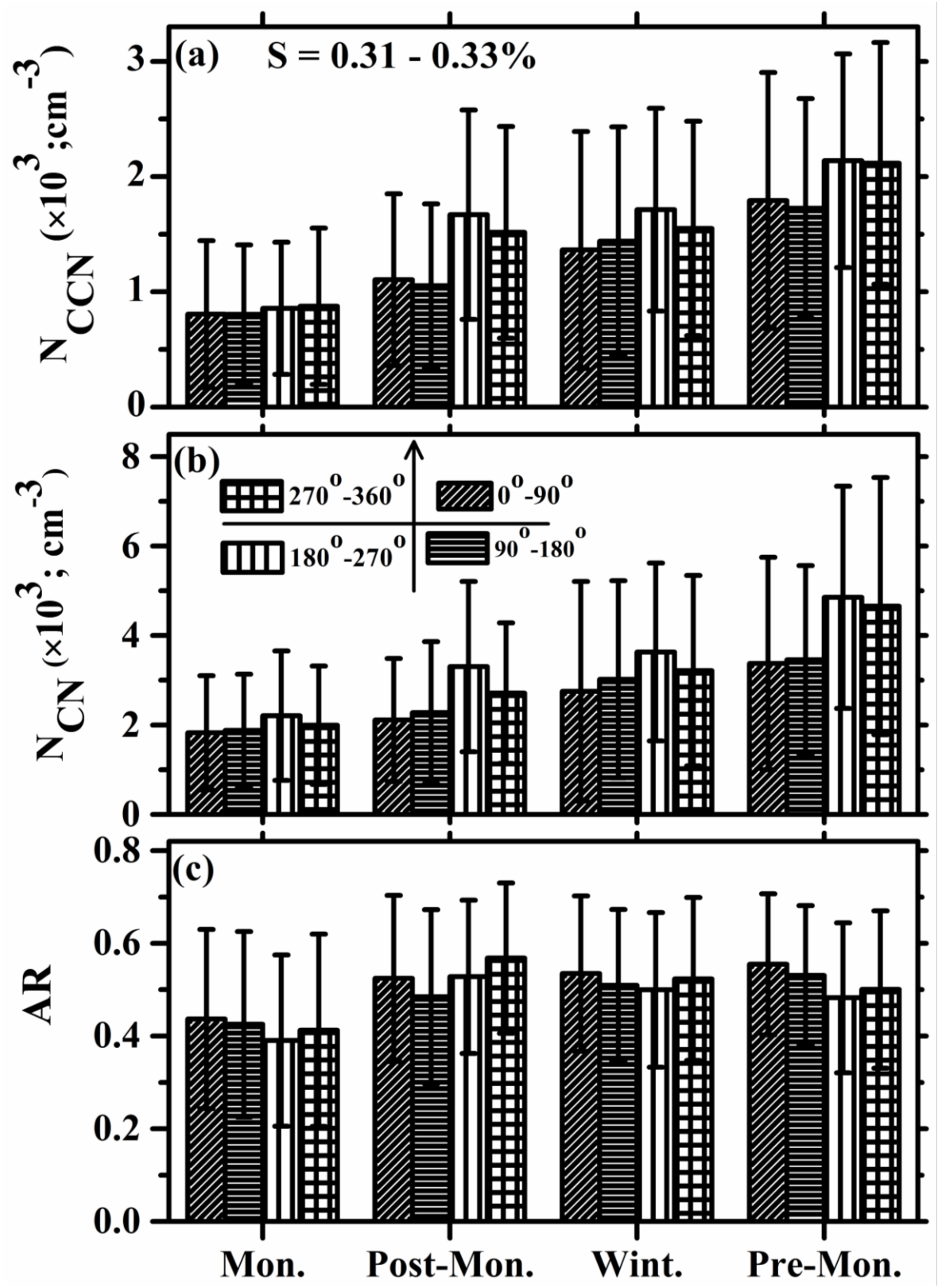
(a) S = 0.31 - 0.33%
N_{CCN} ($\times 10^3$;cm^{-3})
(b)
270°-360°
0°-90°
180°-270°
90°-180°
N_{CN} ($\times 10^3$; cm^{-3})
(c)
AR
Mon.
Post-Mon.
Wint.
Pre-Mon.

Figure 8

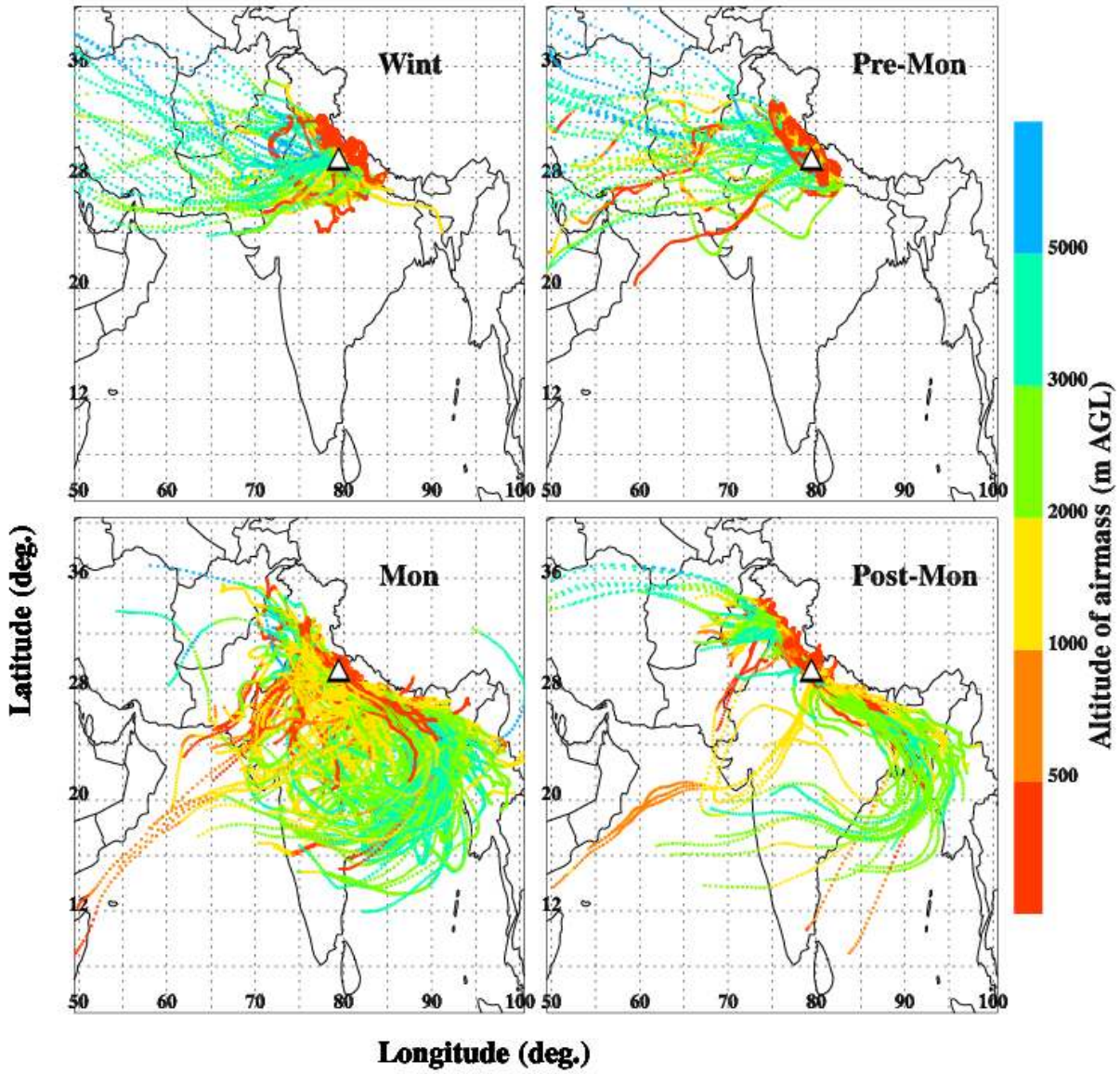
Wint
Pre-Mon
Mon
Post-Mon
Latitude (deg.)
Longitude (deg.)
Altitude of airmass (m AGL)
5000
3000
2000
1000
500

Figure 9

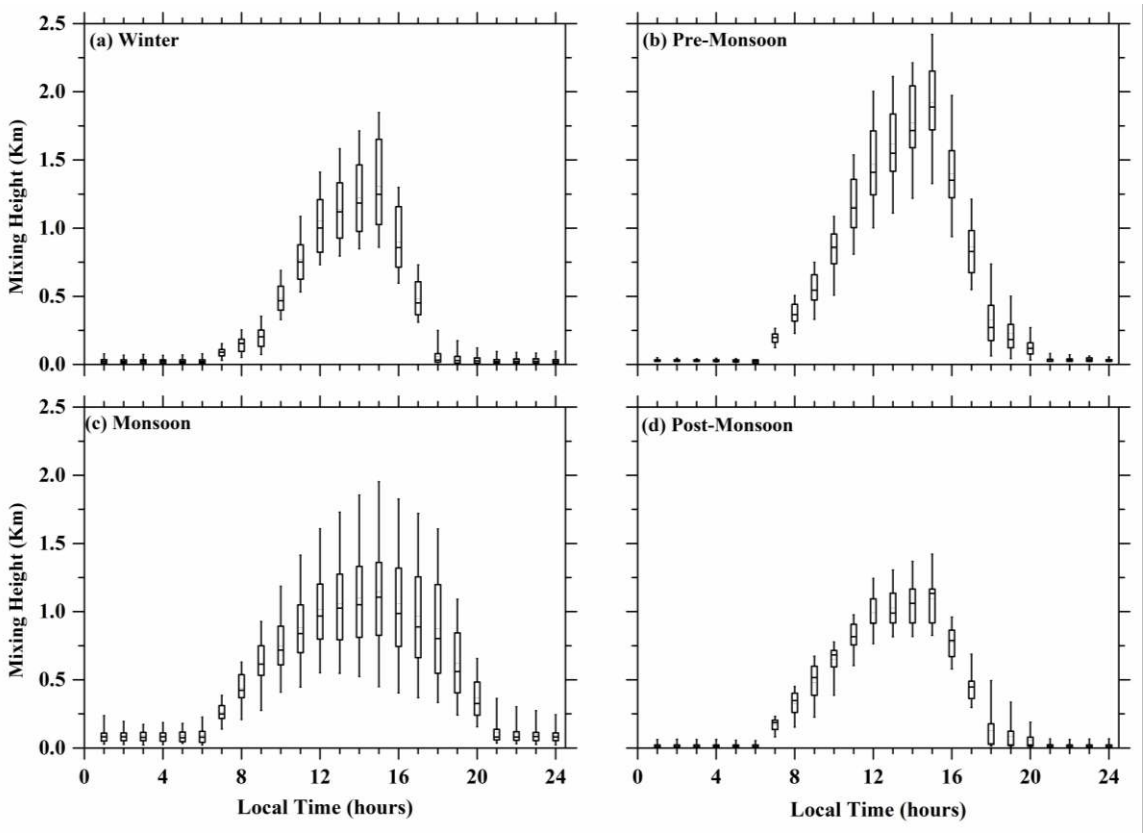
(a) Winter
(b) Pre-Monsoon
(c) Monsoon
(d) Post-Monsoon
Mixing Height (Km)
Local Time (hours)
0.0
0.5
1.0
1.5
2.0
2.5
0
4
8
12
16
20
24

Figure 10

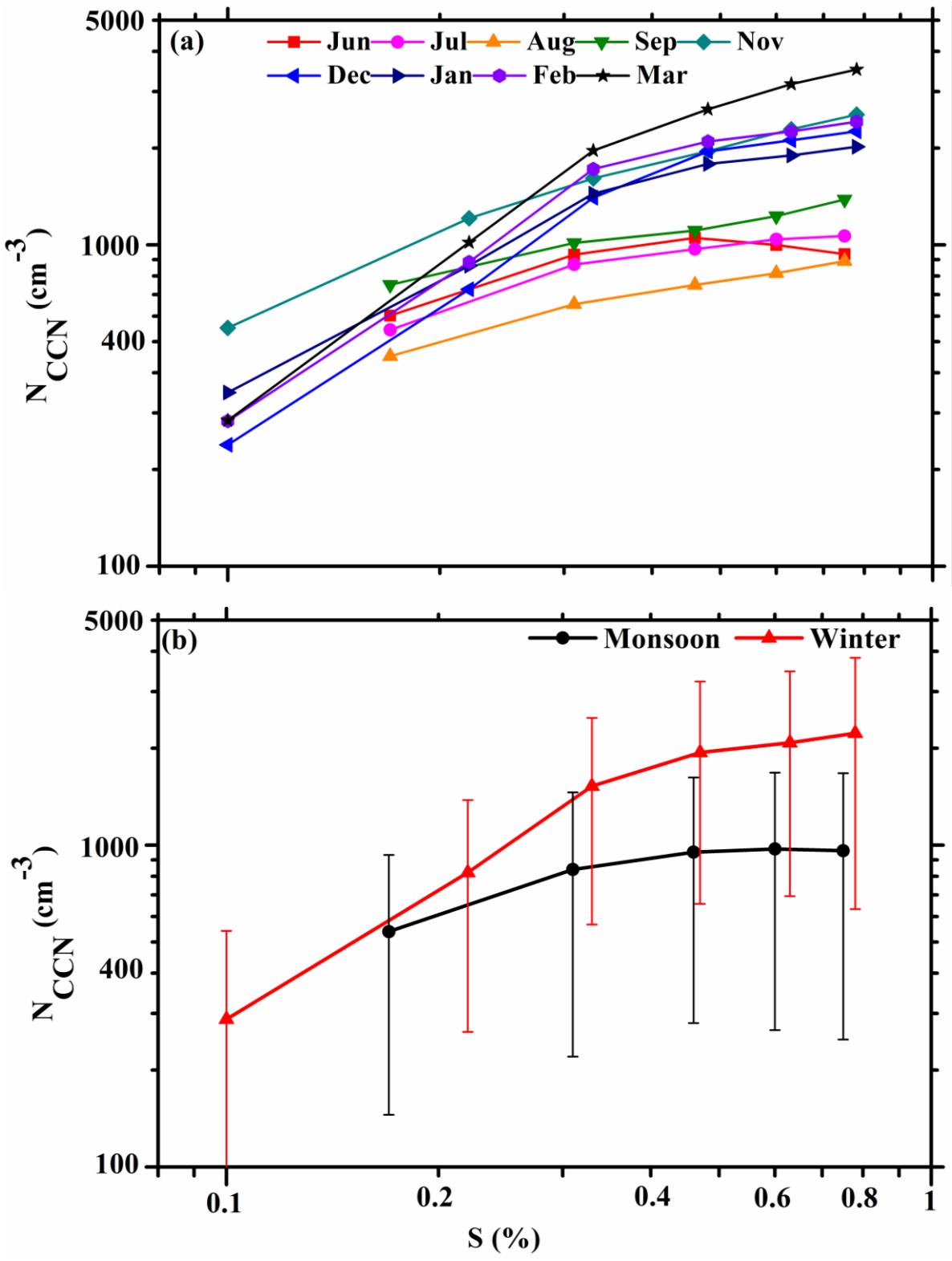
(a)
Jun
Jul
Aug
Sep
Nov
Dec
Jan
Feb
Mar
5000
1000
400
100
N_CCN (cm^-3)
(b)
Monsoon
Winter
5000
1000
400
100
N_CCN (cm^-3)
0.1
0.2
0.4
0.6
0.8
1
S (%)

Figure 11

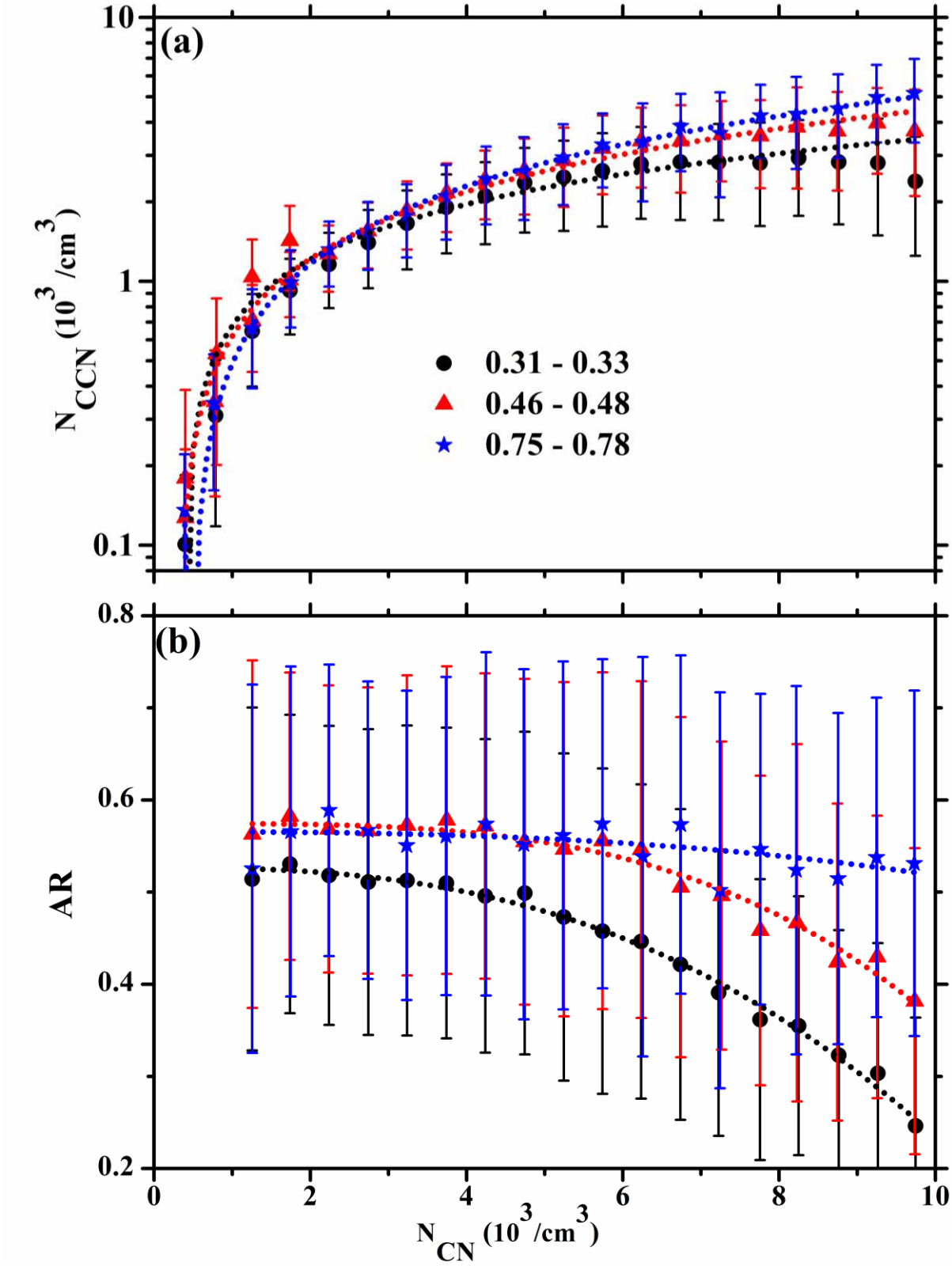
(a)
10
1
0.1
N_{CCN} (10^3 /cm^3)
0.31 - 0.33
0.46 - 0.48
0.75 - 0.78
(b)
0.8
0.6
0.4
0.2
AR
0
2
4
6
8
10
N_{CN} (10^3 /cm^3)

Figure 12

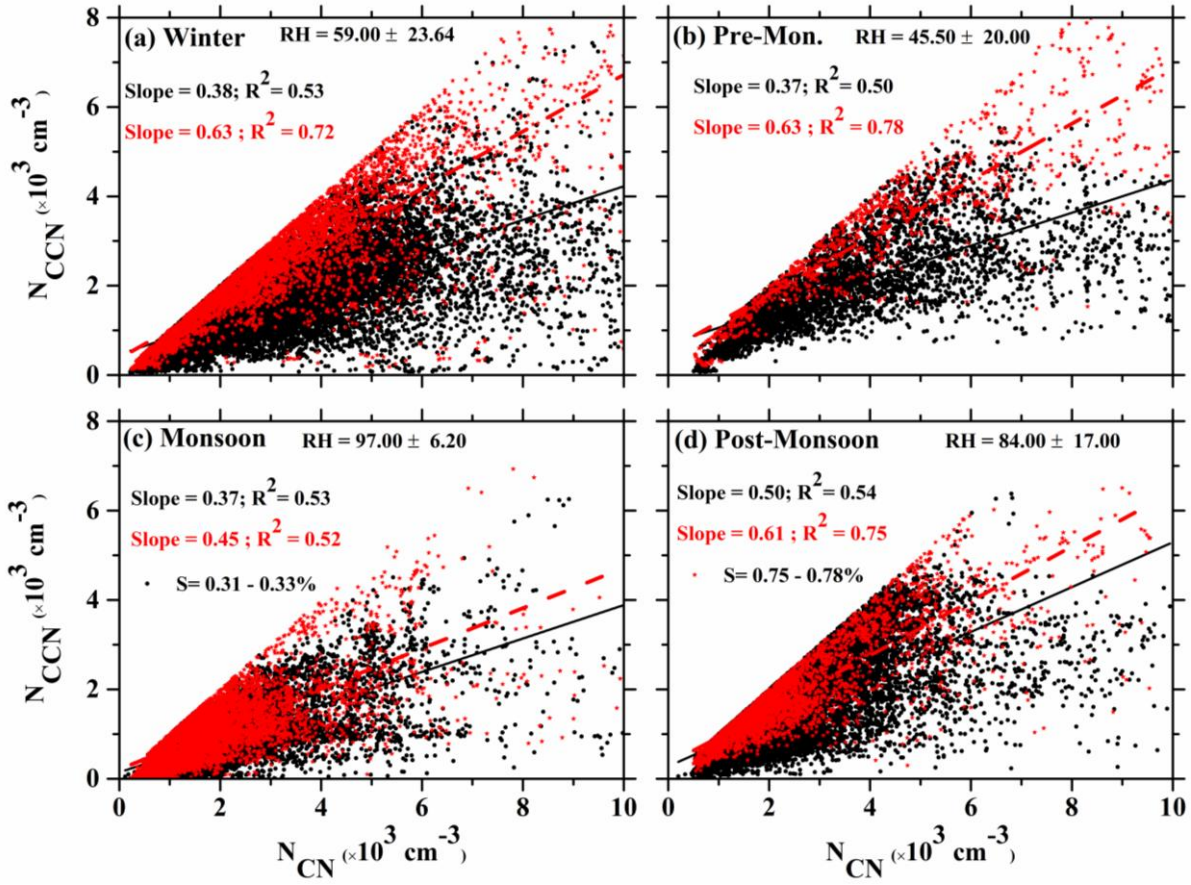
(a) Winter
RH = 59.00 ± 23.64
Slope = 0.38; R2 = 0.53
Slope = 0.63 ; R2 = 0.72
(b) Pre-Mon.
RH = 45.50 ± 20.00
Slope = 0.37; R2 = 0.50
Slope = 0.63 ; R2 = 0.78
(c) Monsoon
RH = 97.00 ± 6.20
Slope = 0.37; R2 = 0.53
Slope = 0.45 ; R2 = 0.52
S= 0.31 - 0.33%
(d) Post-Monsoon
RH = 84.00 ± 17.00
Slope = 0.50; R2 = 0.54
Slope = 0.61 ; R2 = 0.75
S= 0.75 - 0.78%
NCCN (×10^3 cm^-3)
NCN (×10^3 cm^-3)

Figure 13

92

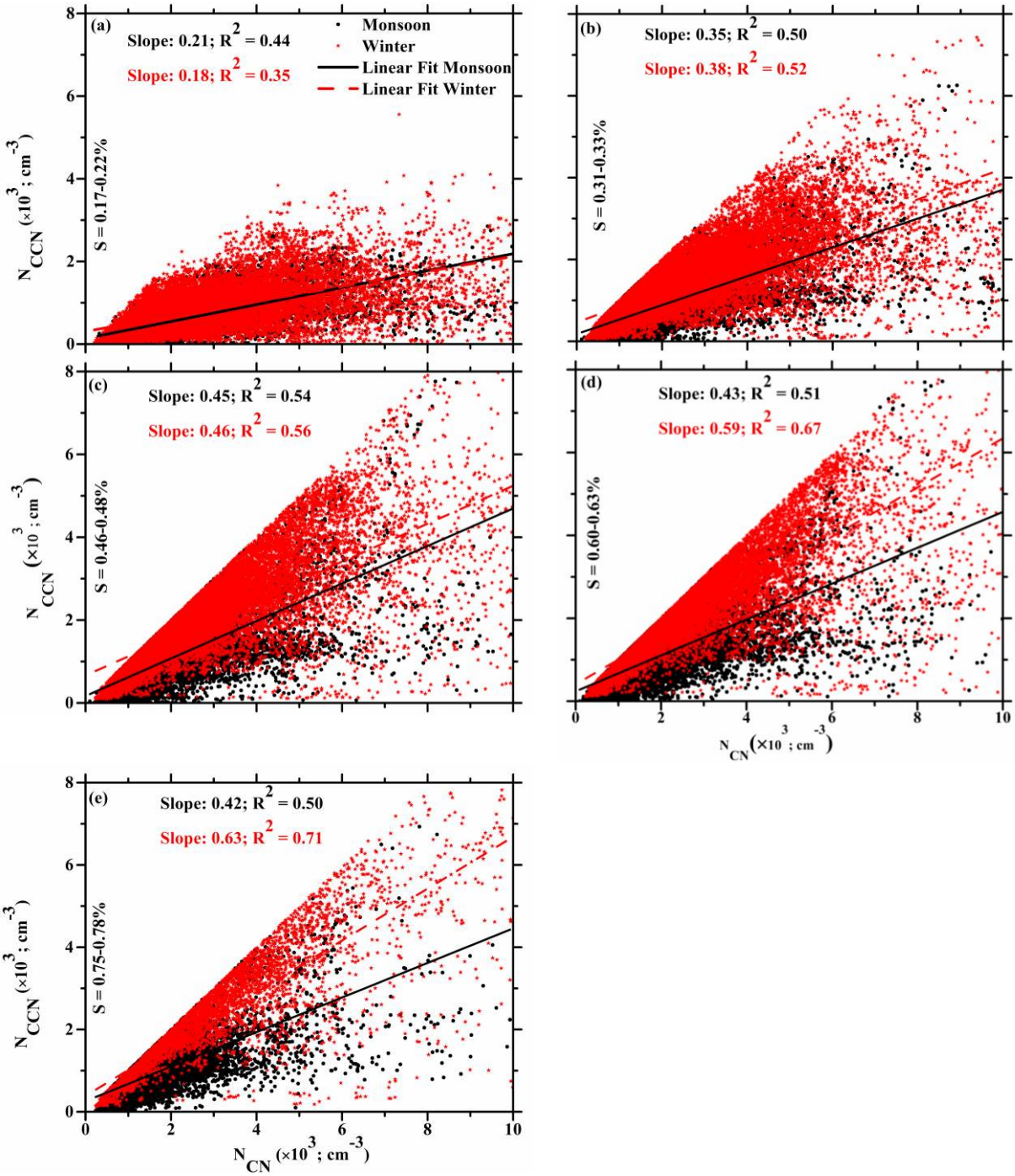

93 **Figure 14**

94

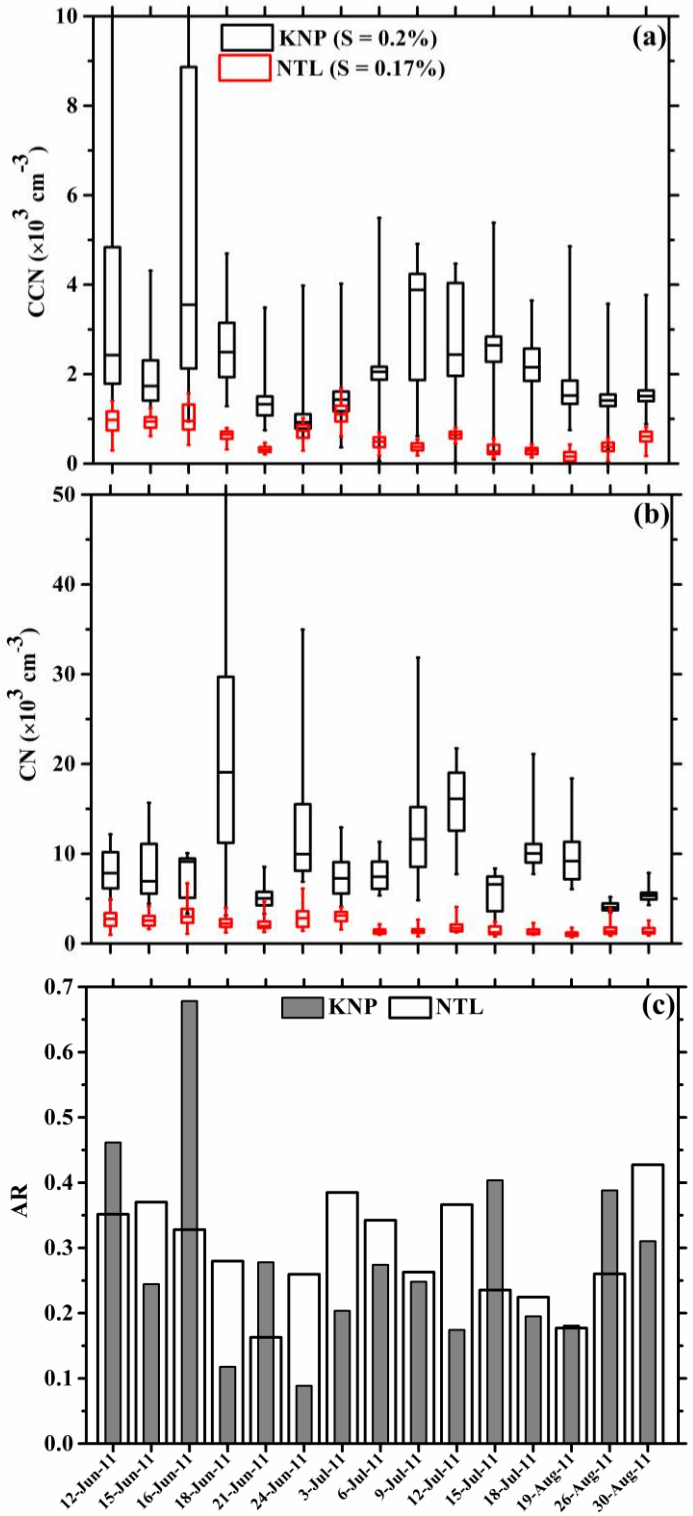
KNP (S = 0.2%)
NTL (S = 0.17%)
(a)
CCN (×10^3 cm^-3)
(b)
CN (×10^3 cm^-3)
KNP
NTL
(c)
AR
12-Jun-11
15-Jun-11
16-Jun-11
18-Jun-11
21-Jun-11
24-Jun-11
3-Jul-11
6-Jul-11
9-Jul-11
12-Jul-11
15-Jul-11
18-Jul-11
19-Aug-11
26-Aug-11
30-Aug-11

Figure 15